Investigating the role of H2A.X di-phosphorylation in the DNA Damage Response

A thesis submitted to the University of Kent for the degree of

M.Sc. Cell Biology in the Faculty of Science, Technology and Medical Studies

2017

Nicola Smith

School of Biosciences

I Declaration

No part of this thesis has been submitted in support of an application for any degree or qualification of the University of Kent or any other University or institute of learning.

Nicola Smith

July 2017

II Acknowledgements

My sincere gratitude goes to my supervisor, Dr. Peter Ellis, without whom this project would not have been possible. I would like to thank him for kindness and compassion, his help and advice, and for answering my endless questions… in detail! I would also like to thank Dr. Claudia Rathje for all her assistance, as well as Professor Darren Griffin and my other good friends in his lab, with whom we share workspace. An additional thanks to my co-supervisor, Professor Martin Michaelis, for also making this project possible.

Collaboration with other laboratories in the School of Biosciences has also greatly assisted this project. In particular, Matthew Badham from the Rossman lab, for providing the cell lines; the Toseland lab for their assistance with the nuclear extraction protocol; the Michaelis lab for teaching me the MTT assay protocol; and the Brown lab for allowing me the endless use of their cooled centrifuge!

Last, but not least, I would like to thank my wonderful family for their eternal support.

III Contents

IV List of Figures

V Abbreviations

293T	Human embryonic kidney cells (HEK-293T)
53BP1	p53-binding protein 1
APAF-1	Apoptotic protease-activating factor 1
ATM	Ataxia telangiectasia-mutated
ATR	Ataxia telangiectasia and Rad3-related protein
BER	Base excision repair
BRCA1	Breast cancer type-1 susceptibility protein
BRCT	BRCA1 C-terminal domains
CAD	Caspase-activated deoxyribonuclease
CSK buffer	Cytoskeleton buffer
DAPI	4',6-diamidino-2-phenylindole hydrochloride
DDR	DNA damage response
Di-γH2A.X	H2A.X phosphorylated at serine-139 and tyrosine-142
DMEM	Dulbecco's Modified Eagle Medium
DNA-PK	DNA-dependent protein kinase
DSBs	Double strand breaks
DDR	DNA damage repair

ER	Endoplasmic reticulum
EYA	Eyes absent protein tyrosine phosphatase
Fas-L	Fas-ligand
γ-H2A.X	H2A.X phosphorylated at serine-139
HAD	Haloacid dehalogenase
HA-tagged	Haemagglutinin-tagged
HSP	Heat shock protein
HP1	Heterochromatin protein 1
HR	Homologous recombination
EDTA	Ethylenediaminetetraacetic acid
HR	Homologous recombination
IR	Ionising radiation
IRIF	Irradiation-induced foci
JNK-1	c-Jun N-terminal kinase-1
MEF	Mouse embryonic fibroblasts
MeCP2	Methyl-CpG-binding protein 2
MCPH1	Microcephalin protein
MDC1	Mediator of DNA damage checkpoint protein 1
MRN complex	MRE11–RAD50–NBS1 protein complex

MTT	3-(4,5-dimethyl-2-thiazolyl)-2,5-diphenyl-2H-tetrazolium-bromide
NER	Nucleotide excision repair
NHEJ	Nonhomologous end joining
pNPP	p-Nitrophenylphosphate
pS139	Phosphorylated H2A.X at serine-139
pY142	Phosphorylated H2A.X at tyrosine-142
PARP1	Poly (ADP-ribose) polymerase 1
PIKK	Phosphatidylinositol 3-kinase-related kinases
PIPES	Piperazine-N,N′-bis(2-ethanesulfonic acid)
PTP	Protein tyrosine phosphatase
ROS	Reactive oxygen species
siRNA	Small interfering RNA
TdT	Terminal deoxynucleotidyl transferase
TNF	Tumour necrosis factor
TRAIL	TNF-related apoptosis-inducing ligand
WICH complex	WSTF-ISWI ATP-dependent chromatin-remodelling complex
WSTF	Williams-Beuren syndrome transcription factor

VI Abstract

One of the earliest responses to DNA double strand breaks is phosphorylation of the C-terminal tail of histone variant H2A.X at position S139. The phosphorylated form (γH2A.X) is a marker of DNA damage and promotes DNA damage repair (DDR). Recent work showed that H2A.X can also be phosphorylated at position Y142, and that increasing Y142 phosphorylation by siRNA knockdown of the Eyes Absent (Eya) phosphotyrosine phosphatases (which remove Y142 phosphates) leads to increased apoptosis in response to DNA damage. This led to the proposal that an epigenetic “switch” between mono-γH2A.X (S139 only phosphorylated) and di-γH2A.X (S139 and Y142 both phosphorylated) directs the choice between DNA repair vs apoptosis in response to DNA damage. In this study, we sought to test this “switch” hypothesis by testing for cooperativity between the DNA damaging drug, Bleomycin, and Benzbromarone – a pharmacological inhibitor of Eya phosphatases. Although little cooperativity between Bleomycin and Benzbromarone was found in cell proliferation assays, live-cell imaging with fluorescent markers of apoptosis showed an increase in cell death. Moreover, by using novel antibodies that specifically recognise the various phosphorylated forms of H2A.X, immunochemical staining revealed that di-γH2A.X is located adjacent to and “flanks” γH2A.X in DDR foci, and is interspersed with γH2A.X in apoptotic cells. Therefore, contrary to the “switch” hypothesis being the singular function of di-γH2A.X, these results suggest an additional model for the role of di-γH2A.X in DDR, in that it may also act as a limiting factor in the rate of expansion of γH2A.X repair foci.

1 Introduction

1.1 Histones and H2A.X

1.1.1 Chromatin structure and function

To facilitate the accommodation of ~2m of DNA inside the ~10μm nucleus of a human cell, the genome is tightly compacted into the highly conserved chromatin structure (Kinner *et al.*, 2008). The basic unit of chromatin is the nucleosome, consisting of a ~100 kDa octamer of highly basic histone proteins, around which 147 bps of the DNA double helix is wrapped in a left-handed superhelical turn (~1.7 times) (Bao, 2011).

The histone octamer is comprised of two copies each of four, small core histone proteins: H2A, H2B, H3, H4, and a linker histone protein, H1. Core histones H2A and H2B associate as a dimer and histones H3 and H4 associate as a tetramer; one H3-H4 tetramer then associates with two H2A-H2B dimers to form the complete octamer (Luger, Dechassa and Tremethick, 2012).

In the primary chromatin structure, nucleosomes are separated by short linker-DNA segments (20-80 bps); termed the 'beads-on-a-string' organisation, chromatin then undergo higher levels of condensation to form the secondary chromatin structure (a 30nm fibre), mediated by interaction between N-terminal domains of adjacent nucleosomes, as well as through non-histone proteins (Luger, Dechassa and Tremethick, 2012).

Higher order tertiary structures are then formed through fibre-fibre interactions and stabilised by histone H1, as well as architectural proteins such as heterochromatin protein 1 (HP1), poly (ADP-ribose) polymerase 1 (PARP1), and methyl-CpG-binding protein 2 (MeCP2) (Luger, Dechassa and Tremethick, 2012) (Figure 1-1).

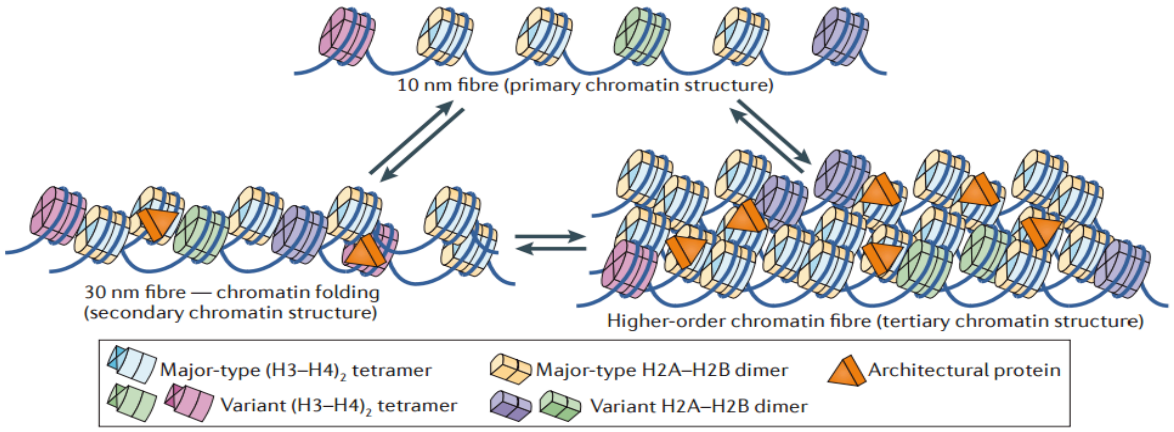

Figure 1-1 Structure of chromatin

Nucleosomes form the primary structure of chromatin, known as the 'beads-on-a-string' organisation. Interactions between adjacent nucleosomes leads to higher levels of condensation, forming a 30nm fibre (secondary structure). Fibre-fibre interactions and stabilisation by scaffold proteins leads to the highly condensed, tertiary chromatin structure (Luger, Dechassa and Tremethick, 2012).

The chromatin structure allows not only the compaction of DNA, but also regulates the accessibility to the genome during transcription, replication, and repair. This structure can be dynamically altered to facilitate or repress the access to DNA, enabled by mechanisms such as ATP-dependent chromatin remodelling complexes, histone variant incorporation, and histone covalent modifications (Bao, 2011); chromatin remodelling complexes can also remove or exchange nucleosomes (Hargreaves and Crabtree, 2011).

1.1.2 Histone variants

The substitution of core histones with histone variants at specific sites can generate a functionally and architecturally distinct chromatin structure. The histone variants are highly conserved between species, indicating that they have specific functions that the canonical histones cannot fulfil (Luger, Dechassa and Tremethick, 2012).

Their expression is replication independent and therefore, unlike the expression of canonical histones that are encoded by replication-coupled genes, histone variants are not restricted to the S-phase of the cell cycle (Henikoff, Furuyama and Ahmad, 2004). Histone variant incorporation often involves ATP-dependent chromatin remodelling factors and specific histone chaperones; an example of which is the exchange of H2A with H2A.Z at specific chromosome locations, facilitated by the ATP-dependent SWR1 complex (Mizuguchi *et al.*, 2004). H2A.Z has also been found to be incorporated near silenced regions of the genome, inhibiting the spread of silent heterochromatin (Meneghini, Wu and Madhani, 2003).

1.1.3 Post-translational modifications of histones

The flexible histone tails extend away from the nucleosomal DNA and are the sites at which many post-translational modifications to amino acid side chains occur, facilitated by several families of catalytic enzymes (Chen *et al.*, 2013).

These modifications include phosphorylation, methylation, acetylation, biotinylation, ubiquitylation, SUMOylation, and ADP-ribosylation; they serve to alter electrostatic interactions between DNA and histones, facilitating the accessibility of cellular functions and changing the dynamics of chromatin (Hunt *et al.*, 2013).

Many of these modifications occur constitutively in undamaged regions of DNA/chromatin and several studies have found that some of these pre-existing modifications have important roles in facilitating the recruitment of DNA damage repair proteins during the DNA damage response (DDR). This includes the finding that either the methylation of histone H3 at lysine-79 (H3K79) or the di-methylation of histone H4 at lysine-20 (H4K20me2) is required for focus formation of the DNA repair protein, p53-binding protein 1 (53BP1) (Huyen *et al.*, 2004; Botuyan *et al.*, 2006). Furthermore, it has been found that post-translational modification of histones in regions of transcriptionally active genes is coupled to preferential DNA double strand break repair (Chaurasia *et al.*, 2012).

One of the best characterised post-translational modifications that occurs in response to DSBs is the phosphorylation of serine-139 (S139) on the C-terminal of histone variant H2A.X, referred to as γH2A.X (Pilch *et al.*, 2003). In addition, it has been found that phosphorylation of the N-terminal of H4 at serine-1 (Cheung *et al.*, 2005), and H2B at serine-14 (Fernandez-Capetillo, Allis and Nussenzweig, 2004), also occur in the DDR.

1.1.4 H2A.X

H2A.X is one of the most conserved variants of H2A; it differs from H2A in that it has an extended C-terminal tail (an additional 14 amino acids), on which there is an SQEY motif. The primary sequence of H2A.X is different from H2A in just four amino acids: Q6T, T16S, N38H and K99G (Bonisch and Hake, 2012). It is ubiquitously expressed in all cell types and represents between 2-25% of the H2A complement in mammals (Rogakou *et al.*, 1998; Kinner *et al.*, 2008).

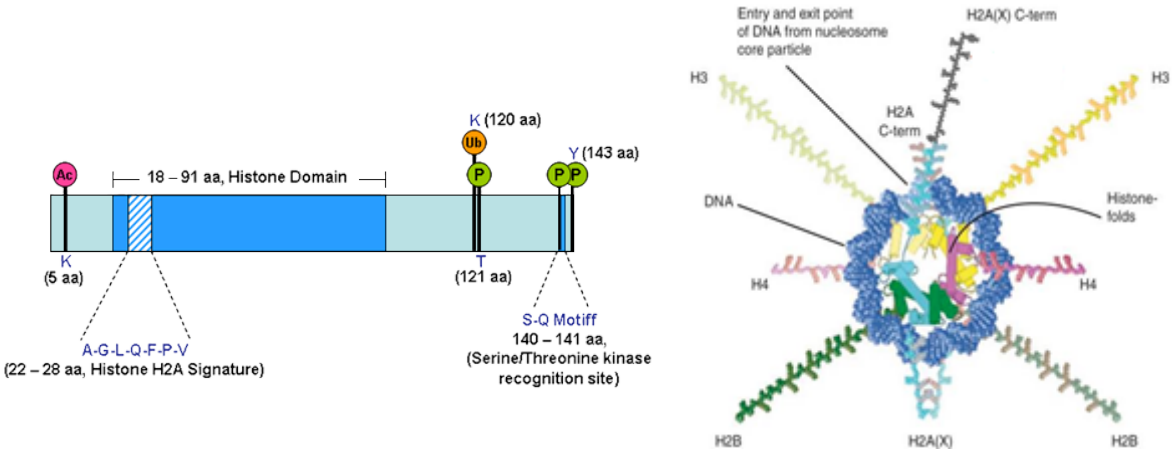

Figure 1-2 Structure of histone H2A.X and model of the nucleosome core

H2A.X has a characteristic H2A domain, which ranges from 18-91 amino acids (aa) that contains the 22-28aa H2A signature motif. H2A.X differs from H2A in that it has an extended C-terminus containing the SQEY-motif (residues 140-143) (left). A schematic drawing (right) of the DNA interaction with the histone octamer and histone tails, including that of histone variant, H2A.X (*H2AFX (H2A histone family, member X);* Kinner *et al.*, 2008)**.**

Since the discovery that exposure to ionising radiation results in γH2A.X formation, as part of the DDR (Rogakou *et al.*, 1998), it has been the subject of many subsequent studies.

A more recent comprehensive screen of H2A.X residues revealed that in addition to phosphorylation, H2A.X is also modified by acetylation, ubiquitylation, and SUMOylation (Chen *et al.*, 2013; van Attikum and Gasser, 2009).

In addition to its more characterised role in the DDR, H2A.X performs a multitude of biological processes, including roles in sex chromosome inactivation in germ cells, X chromosome inactivation in somatic cells, chromatin regulation in mitosis, embryonic stem cell development, neural stem cell development, asymmetric sister chromosome segregation, and cellular senescence maintenance (Turinetto and Giachino, 2015).

1.2 H2A.X in the DNA Damage Response

1.2.1 DNA damage

Cells are constantly exposed to endogenous and exogenous stresses that induce a multitude of DNA lesions, of which many thousands arise every day in mammalian cells (Polo and Jackson, 2011). Endogenous stresses come from essential metabolic activity, such as oxidative respiration and lipid peroxidation that generate reactive oxygen species (ROS); exogenous stresses come from numerous environmental agents such as ionising radiation (IR) and ultraviolet (UV) light, as well as genotoxic chemicals that are present in combustion products and food (Dinant, Houtsmuller and Vermeulen, 2008; Iliakis, Murmann and Soni, 2015).

These potentially harmful DNA lesions include double strand breaks (DSBs), which can also occur as intermediates during meiotic and V(D)J recombination (Khanna and Jackson, 2001), and have to be efficiently repaired in order to prevent genetic rearrangements that can lead to genomic instability, cell death or oncogenic transformation.

1.2.2 Repair of DNA damage

Erroneous DNA repair can lead to chromosomal aberrations, therefore eukaryotic cells have evolved an elaborate system for DNA damage detection to prevent the transmission of this genetic instability to their offspring; this involves regulating access to the site of damage through chromatin structure alterations, the coordination with cell-cycle checkpoints, and arrest of cell-cycle progression (Torgovnick and Schumacher, 2015). DNA damage therefore initiates a complex cascade of cell signalling, chromatin modification, and repair events.

DSBs are among the most toxic of DNA lesions and can be induced by IR in all phases of the cell cycle. The repair of these is therefore critical as incorrect repair of such lesions can lead to chromosomal translocations; whereas left unrepaired, these lesions can result in cells undergoing apoptosis or senescence, or the loss of chromosome fragments causing the potential loss of essential tumour suppressor genes (Davis and Chen, 2013; van Gent and Kanaar, 2016).

There are at least four major pathways that have evolved to deal with the many different types of DNA lesions that occur: base excision repair (BER), nucleotide excision repair (NER), non-homologous end joining (NHEJ), and homologous recombination (HR). Small, non-helix distorting base lesions are excised and replaced by BER (Caldecott, 2007; Kim and Wilson, 2012); whereas NER is able to target may different types of single-strand breaks that destabilise the structure of the double helix, including the cyclobutene pyrimidine dimers and 6-4 photoproducts induced by UV, as well as large or bulky chemical adducts (Schärer, 2013).

The more harmful lesions caused by DSBs are dealt with by HR and NHEJ (Dinant, Houtsmuller and Vermeulen, 2008): HR utilises the presence of a homologous template, usually a sister chromatid, to make an accurate repair and this method is therefore predominantly post-replicative in the S- and G2-phase of the cell-cycle (Li and Heyer, 2008); whereas whilst NHEJ can also target DSBs in S-phase, this is a more error prone repair mechanism that operates mainly in G1-phase and utilises the Ku heterodimer (Ku70 and Ku80 proteins) to directly ligate DNA ends, with minimal processing (Davis and Chen, 2013).

1.2.3 Role of γH2A.X in the DNA Damage Response

During the process of sensing DNA damage and subsequent repair, histones undergo post-translational modifications to be able to direct the recruitment of DNA repair proteins. These modifications include phosphorylation, ubiquitylation,

methylation, and acetylation; these also serve to assist the restoration of chromatin to its native state following repair (van Attikum and Gasser, 2009; Hunt *et al.*, 2013; Chen *et al.*, 2013). In response to DSBs, H2A.X is phosphorylated on its carboxy-terminal tail, at S139, by phosphatidylinositol 3-kinase-related kinases (PIKKs) such as ataxia telangiectasia-mutated (ATM), ataxia telangiectasia and Rad3-related protein (ATR), and DNA-dependent protein kinase (DNA-PK), to form long stretches of γH2A.X that flanks the DSBs; this occurs within minutes following exposure to IR (Pilch *et al.*, 2003; Cook *et al.*, 2009; Zhu *et al.*, 2011). γH2A.X forms a domain that extends up to 50 kilobases either side of the DNA damage in yeast (Shroff *et al.*, 2004), and several mega-bases in mammals (Rogakou *et al.*, 1999). This leads to the recruitment of DNA damage repair proteins such as the mediator of DNA damage checkpoint protein 1 (MDC1), p53-binding protein 1 (53BP1), the breast cancer type-1 susceptibility protein (BRCA1), and the MRE11–RAD50–NBS1 (MRN) complex (van Attikum and Gasser, 2009).

In addition, the formation of γH2A.X also facilitates the recruitment of chromatin remodelling complexes, such as RSC and SW1/SNF (Park *et al.*, 2006), as well as other repair proteins belonging to the SWI2/SNF2 family of dsDNA-dependent ATPase helicases that are involved in the DDR, such as RAD5, RAD16, RAD54 and CSB/RAD26 (Ceballos and Heyer, 2011; Ortiz-Bazán *et al.*, 2014); thus H2A.X is a central player in the DDR and therefore deficiency is linked to decreased genomic stability and an increased susceptibility to tumour development in normal cells and tissues (Zhu *et al.*, 2011).

The finding that the MRN complex protein, NBS1, binds to and activates the ATM kinase provides a model for how MDC1 is able to extend phosphorylation of H2A.X over large regions of chromatin (van Attikum and Gasser, 2009). Specifically, the MRN complex recognises and binds to DSBs (Petrini and Stracker, 2003), this then recruits ATM through an interaction with the C-terminus of NBS1 (You *et al.*, 2005). This recruitment of ATM leads to phosphorylation of H2A.X (Burma *et al.*, 2001) and subsequent recruitment of MDC1. This in turn promotes the recruitment and retention of further MRN complex proteins, promoted by the phosphorylation of MDC1 by casein kinase 2 (CK2) (Spycher *et al.*, 2008); thus more ATM is recruited through interaction with NBS1 and provides a positive feedback mechanism which allows the extension of γH2A.X to surrounding chromatin (Figure 1-3). This signal amplification allows for transmission of a localised DNA repair process to activation of cell-cycle checkpoint and arrest signalling (Misteli and Soutoglou, 2009).

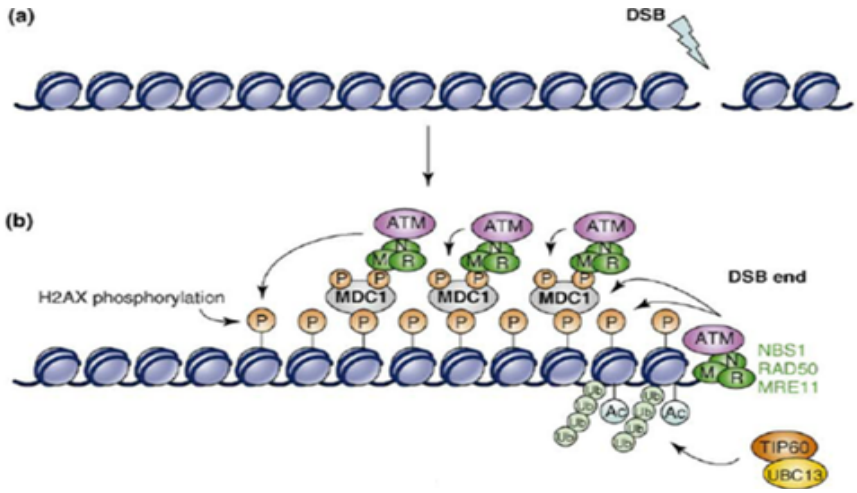

Figure 1-3 Initiation of repair foci in the DNA Damage Response

(a) Induction of DSB (b) The MRN complex binds to the ends of DSBs and recruits ATM. ATM phosphorylates H2A.X, leading to recruitment of MDC1. MDC1 recruits further MRN complexes, and in turn further ATM. ATM phosphorylates proximal H2A.X, allowing spread of γH2A.X to surrounding chromatin. TIP60 acetylates γH2A.X which initiates γH2A.X polyubiquitylation by UBC13 for γH2A.X removal (adapted from van Attikum and Gasser, 2009).

1.2.4 Apoptosis

1.2.4.1 Overview

Programmed cell death is an evolutionary conserved process that has distinct morphological characteristics (Kerr, Wyllie and Currie, 1972). It plays an important role in both the development of multicellular organisms, such as tissue sculpting in embryonic development; maintenance of tissue homeostasis by the elimination of cells in normal turnover as well as those that are potential harmful; and through chemically induced cell death (Elmore, 2007; Nagata, 2010). The deregulation of apoptosis therefore has implications in many diseases, including autoimmune disease and cancer (Solier and Pommier, 2014).

Apoptosis can be triggered by various stimuli, including endoplasmic reticulum (ER) stress, oxidative stress, irradiation, and chemotherapeutic agents (Ichim and Tait, 2016). There are two distinct pathways that initiate the first stage of apoptosis, cell death: extrinsic apoptosis is initiated by the death receptor mediated pathway, by ligands such as tumour necrosis factor (TNF) and TNF-related apoptosis-inducing ligand (TRAIL) at the cell surface; whereas intrinsic apoptosis is initiated by the mitochondrial pathway (Murphy, Perry and Lawler, 2008).

Caspases are a family of aspartate-specific cysteine proteases that are synthesised as inactive proenzymes. These act as death effector molecules upon activation, causing a sequential activation of downstream caspase zymogens (Taylor, Cullen and Martin, 2008). During the extrinsic apoptotic pathway, the

ligand binding initiates the recruitment of adapter proteins and molecules of the initiator caspases (procaspase-8 and -10) to the cytosolic face of the death receptor (Zhao, Sui and Ren, 2010). Cleaved, activated initiator caspases then propagate the signal through proteolytic activation of downstream executioner caspases: caspase -3, -6 and -7 (Wachmann *et al.*, 2010).

A dynamic equilibrium exists in the BCL-2 family members, which consist of pro- and anti-apoptotic proteins; these play key roles in the mitochondrial-mediated apoptotic pathway which can arise from a number of stimuli, including DNA damage (Ichim and Tait, 2016). Pro-apoptotic proteins translocate to the mitochondria where they negate the protective activity of anti-apoptotic proteins, thereby causing membrane permeabilisation and an efflux of pro-apoptotic proteins such as cytochrome c into the cytosol (Nagata, 2010). Cytochrome c then binds to apoptotic protease-activating factor 1 (APAF-1) and together with the initiator caspase-9 forms the apoptosome, which leads to activation of the executioner caspases -3, -6 and -7 (Bratton and Salvesen, 2010).

Apoptosis is characterised by a series of typical morphological and biochemical features, such as nuclear and cytoplasmic condensation, cell shrinkage, DNA “laddering” due to its degradation by caspase-activated deoxyribonuclease (CAD), fragmentation into membrane-bound apoptotic bodies, and is followed by rapid phagocytosis by neighbouring cells for degradation and recycling (Kerr, Wyllie and Currie, 1972; Nagata *et al.*, 1998).

1.2.4.2 γH2A.X in apoptosis

In 2009, Solier and colleagues discovered a novel pattern of γH2A.X staining during early apoptosis, detected by immunofluorescence microscopy. They used both cancer cells and normal cells and induced apoptosis by subjecting them to treatment with either agonists of the death receptor pathway, TRAIL and Fas-ligand (FasL), or by using the apoptosis initiator, Staurosporine (Solier and Pommier, 2009).

They observed that in contrast to the distinct γH2A.X foci pattern that has previously been seen following treatment with IR, which is distributed throughout the nucleus during DDR at sites of DSBs, instead that during early initiation of apoptosis, γH2A.X is visible at the inner face of the nuclear envelope, in a ring-like pattern that they refer to as the “apoptotic ring” (Figure 1-4). This staining pattern was found in both cancer cells and normal cells; it was also observed that after this early phase of apoptosis, pan-staining of the nucleus occurred, followed by pan-staining in the apoptotic bodies (Solier and Pommier, 2009). A later study, by the same group, noted that the apoptotic ring pattern of staining is not restricted to the extrinsic apoptotic pathway; it was also found to be induced by anticancer agents through the intrinsic pathway (Solier and Pommier, 2014).

Interestingly, the same pattern of nuclear peripheral staining was seen when staining for DNA-PK kinase, indicating that in contrast to ATM being the predominant kinase of H2A.X during the DDR, that DNA-PK may represent the

predominant kinase of H2A.X during the extrinsic pathway of apoptosis induction (Solier and Pommier, 2009). They also found that DNA damaging drugs produced two consecutive waves of H2A.X response: a population of cells harbouring γH2A.X damage foci that appeared within the first few hours following 15 Gy of irradiation, followed by a second population of mostly apoptotic pattern stained cells at later times. They also noted that high doses of DNA damaging agents could produce the two populations simultaneously (Solier and Pommier, 2014).

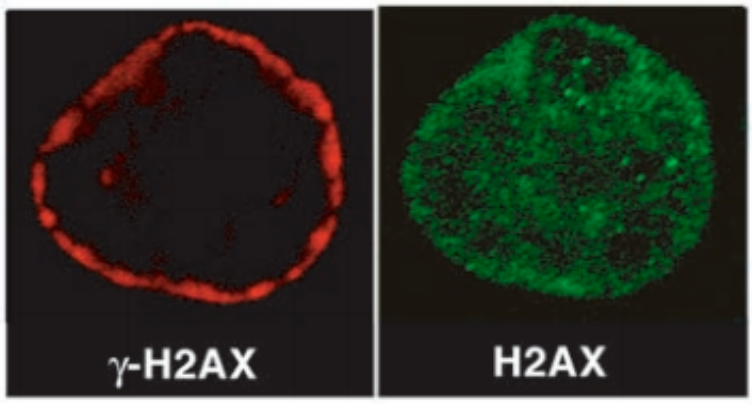

Figure 1-4 Apoptotic ring formation

A human colon carcinoma HCT116 cell following apoptosis induction with the death receptor ligand, TRAIL and stained with antibodies against γH2A.X (left) and total H2A.X (right). Pattern of staining shows the apoptotic ring during early apoptosis, in contrast to uniform distribution of total H2A.X (Solier and Pommier, 2009)

In this study and subsequent studies, the apoptotic ring was found to colocalise with phosphorylated histone H2B (at serine-14), DDR protein kinases CHK2, ATM, DNA-PK, and also with the DNA-PK chaperone, heat shock protein HSP90α, which is required for DNA-PK activation (Solier *et al.*, 2012). Though they found that it did not colocalise with DDR protein 53BP1, suggesting that there may be a different

molecular mechanism of γH2A.X induction during apoptosis, compared to DSB repair (Solier and Pommier, 2009). They subsequently found however, that another one of the key proteins in the DDR, MDC1, is also absent from the apoptotic ring which could potentially explain the absence of 53BP1 (Solier and Pommier, 2011). They went on further to find that during the early phase of apoptosis, MDC1 is cleaved by activated caspase-3, abrogating its interaction with γH2A.X and DDR factors and thus curtailing any further DNA repair (Solier and Pommier, 2011).

A plausible reason for the apoptotic "ring" is that this is formed in response to the DSBs caused by caspase-activated deoxyribonuclease (CAD) during the initiation of apoptosis: CAD is normally sequestered in the cytoplasm as an inactive complex with its inhibitor ICAD, but is released by caspase-3 cleavage during apoptosis and is able to diffuse into the nucleus (Nagata *et al.*, 1998; Rogakou *et al.*, 2000). Interestingly, phosphorylation of H2A.X appears to be necessary for DNA cleavage by CAD (Lu *et al.*, 2006).

1.3 Phosphorylation of H2A.X at Tyrosine 142

1.3.1 WSTF phosphorylates Tyrosine 142

In 2009, studies performed by Xiao and colleagues discovered a novel post-translational modification of H2A.X: they found that the amino-terminal domain of WSTF (Williams-Beuren syndrome transcription factor), a member of the BAZ/WAL family chromatin remodelling factors, could phosphorylate the SQEY motif of H2A.X at tyrosine 142 (Y142).

WSTF forms part of the WICH complex (WSTF-ISWI ATP-dependent chromatin-remodelling complex), believed to be involved in DNA replication and the mobilisation of nucleosomes (Xiao *et al.*, 2009). The study went on to demonstrate that WSTF co-immunoprecipitates with H2A.X, but not with a Y142F mutant; and that small interfering RNA (siRNA) knock down of WSTF significantly reduced the Y142 phosphorylation.

1.3.2 Tyrosine phosphorylation reduces following ionising radiation

To determine a potential role for WSTF and Y142 phosphorylation in the DNA damage response, both wild-type and WSTF RNAi cells were subjected to IR. Interestingly, it was found that in contrast to the large γH2A.X foci that formed at 4hrs post-IR and persisted until 12hrs post-IR in the control cells, large foci failed to form altogether in the WSTF RNAi cells. This was supported by western blot analysis which showed that, in contrast to the increase in γH2A.X seen 1hr post-IR and sustained until 12hrs post-IR in wild-type cells, WSTF RNAi cells had an increase in γH2A.X at 1hr post-IR but that this was not maintained and had sharply decreased by 4hrs post-IR and did not recover (Xiao *et al.*, 2009).

The results of this study therefore suggests that WSTF mediated phosphorylation of Y142 has a vital role in the DDR and is necessary to maintain γH2A.X formation. Furthermore, it suggests that Y142 is constitutively phosphorylated in primary mouse embryonic fibroblast (MEF) cells, and that following IR, pY142 is gradually dephosphorylated (Figure 1-5), although there does appear to be some recovery

after 10hrs. This finding is in part supported by a study by Solier and colleagues (2011), in which they found that TRAIL-induced apoptosis caused a decrease in Y142 phosphorylation and that Y142 was not associated with the apoptotic ring (Solier and Pommier, 2011).

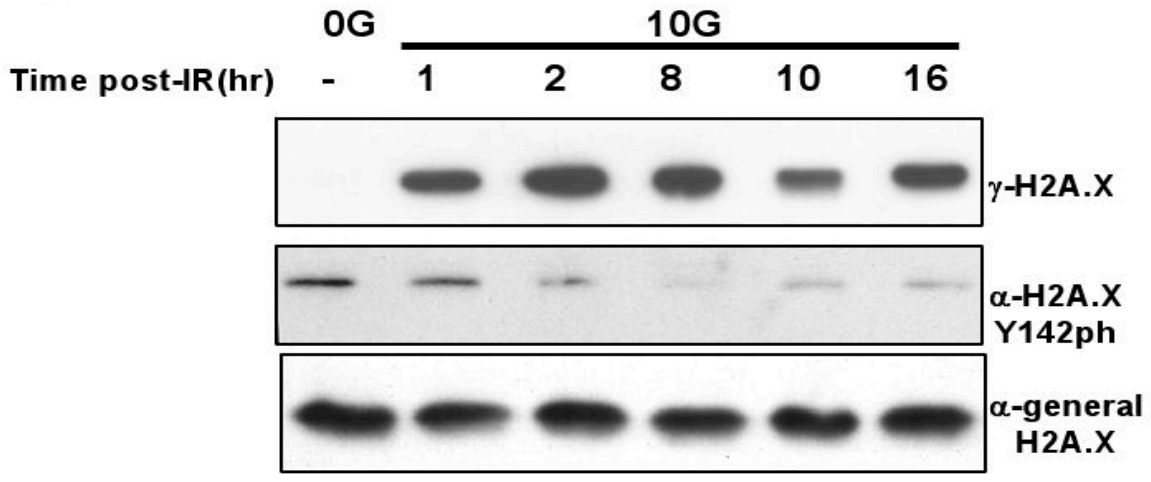

Figure 1-5 Tyrosine 142 is dephosphorylated following ionising radiation
Acid-extracted histones, from primary MEF cells, following 10 Gy of ionisising radiation (IR). Extracts were separated by SDS-PAGE; immunoblotting for γH2A.X, pY142, and general H2A.X as a loading control (Xiao *et al.*, 2009).

1.3.3 Tyrosine 142 dephosphorylation by Eya phosphatase

Where Xiao and colleagues looked at the impact of inhibition of Y142 phosphorylation, Cook and colleagues (2009) investigated the effect of inhibiting the removal of Y142 phosphorylation on the DDR. In particular, they explored the protein tyrosine phosphatase, Eya (Eyes Absent), as a potential phosphatase of Y142.

Co-immunoprecipitation studies were performed using HEK293T (293T) embryonic kidney cells: these showed that both Eya1 and Eya3 interact with H2A.X under DNA damage conditions (IR), but not in control cells. This was supported by immunostaining, which revealed that HA (haemagglutinin)-tagged Eya1 or Eya3 co-localised with γH2A.X following IR (Figure 1-6) (Cook *et al.*, 2009).

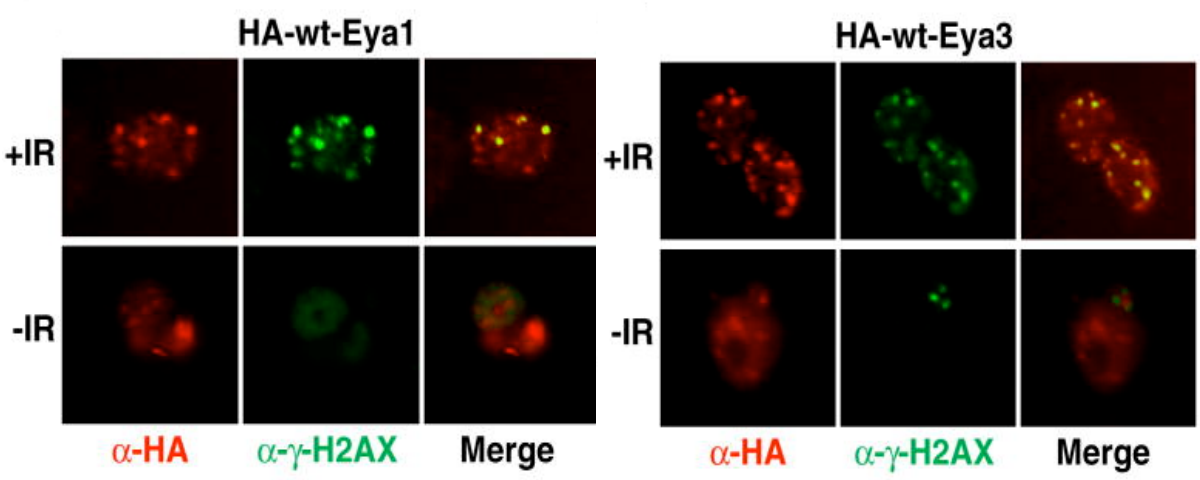

Figure 1-6 Colocalization of Eya1 and Eya3 with γ-H2A.X
HEK293T cells were transfected with HA-tagged EYA1 or EYA3. 1hr following 5 Gy of ionizing radiation, Eya 1/3 co-localises with γH2A.X foci (Cook *et al.*, 2009).

These results suggest that the Eya protein tyrosine phosphatase is recruited to H2A.X foci in response to DNA damage. Their studies further went on to demonstrate that 293T cells, transfected with siRNA against Eya1 or Eya3, showed a significantly increased level of phosphotyrosine. In contrast, control siRNA cells and untransfected cells displayed a loss of H2A.X tyrosine phosphorylation following IR, supporting the data found by Xiao and colleagues (Figure 1-5) (Cook *et al.*, 2009).

In further support of the WSTF RNAi results seen by Xiao and colleagues, Cook and colleagues found that a flag-tagged H2A.X mutant (Y142F) was phosphorylated on S139 at significantly lower levels than the wild-type H2A.X; this promotes the suggestion that Y142 phosphorylation plays an important role in either maintaining or promoting the γH2A.X formation following DNA damage (Cook *et al.*, 2009).

1.3.4 Di-phosphorylation of H2A.X

Cook and colleagues then went on to investigate a connection between Y142 dephosphorylation and the apoptotic response. Consistent with a study that found that MDC1 binds directly to γH2A.X (Stucki *et al.*, 2005), Cook and colleagues used synthetic peptides corresponding to the C-terminal tail of H2A.X that were either phosphorylated at S139 alone (γH2A.X), or di-phosphorylated, (pS139pY142), followed by affinity purification with nuclear extracts from gamma irradiated 293T cells. Intriguingly, they found that repair protein MDC1, and MRN complex proteins (Rad-50 and MREII) interacted with γH2A.X, yet failed to interact with the di-phosphorylated peptides (Figure 1-7).

Furthermore, the di-phosphorylated peptides instead interacted with activated c-Jun N-terminal kinase-1 (JNK-1): an interaction that was not observed with γH2A.X. JNK-1 has been found in previous studies to be involved in the UV induced phosphorylation of H2A.X and associated with the induction of apoptosis (Lu *et al.*, 2006).

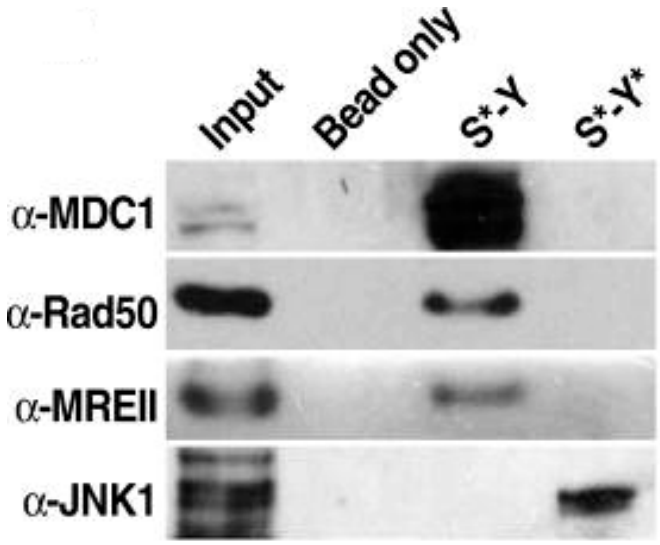

Figure 1-7 Interaction of H2A.X synthetic peptides with either DNA repair proteins or pro-apoptotic proteins

Pull-down study with synthetic peptides representing C-terminal of H2A.X (* depicts a phosphorylated residue): γH2A.X interacts with DNA repair factors (MDC1, Rad50, MRE11), whereas di-phosphorylated H2A.X interacts with the pro-apoptotic protein, JNK-1 (Cook *et al.*, 2009).

Cook and colleagues also used C-terminal peptides that were either unphosphorylated on both residues, or where the terminal tyrosine had been mutated to alanine (Y142A); in both instances, MDC1 failed to make an interaction. This suggests that the unphosphorylated form of Y142 is necessary for MDC1 to form an interaction with γH2A.X. Furthermore, they performed pull-down studies following siRNA knock down of Eya3 and treatment with 10 Gy of radiation: as predicted, there was a loss of interaction between H2A.X and MDC1. This was further corroborated by a fluorescence polarisation spectroscopy study, conducted by Campbell and colleagues, in which they found a greater than 300-fold reduction in the affinity of the MDC1-BRCT domain for γH2A.X, when Y142 was also

phosphorylated. It is therefore suggested that pY142 has a role in blocking the binding of MDC1 to undamaged chromatin (Campbell, Edwards and Glover, 2010).

Finally, Cook and colleagues examined the effect of siRNA knock down of Eya on apoptosis through a TUNEL assay, following subjection of 293T cells to hypoxia treatment. They found that siRNA knock down of either Eya1 or Eya3 caused an increase in apoptotic cell death (Cook *et al.*, 2009).

1.3.5 Proposed model of H2A.X in DDR

In summary of their studies, Cook and colleagues (2009) proposed the following model (Figure 1-8): they postulate that H2A.X is phosphorylated at Y142 at basal levels in undamaged cells. Upon DNA damage, the presence of pY142 becomes critical in making the fundamental decision between DNA damage repair or apoptosis. DNA damage activated ATM kinase then phosphorylates and activates the Eya tyrosine phosphatase: this functions to dephosphorylate Y142 and allows a temporal switch to the mono-phosphorylated form (γH2A.X), thus allowing recruitment of MDC1 and repair mediators to γH2A.X at the site of damage. However, when the C-terminal tail of H2A.X is di-phosphorylated (di-γH2A.X), recruitment of MDC1 is impeded and pro-apoptotic proteins are instead recruited. However, this model was not supported by the findings of Solier and colleagues (2011), in which they found that TRAIL-induced apoptosis caused a decrease in Y142 phosphorylation and that Y142 was not associated with the apoptotic ring, suggesting that it may not be the governing determinant of apoptosis induction.

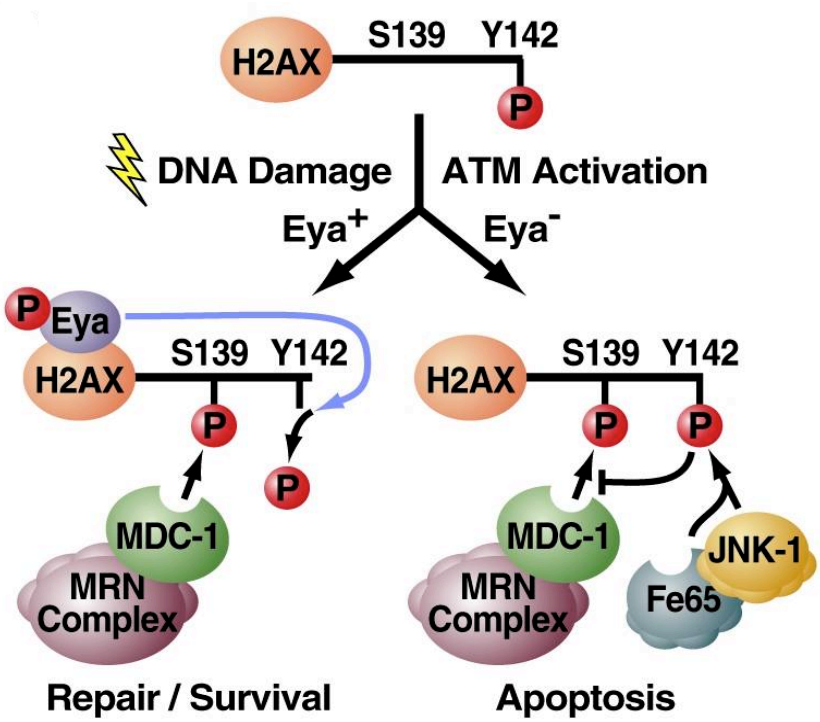

Figure 1-8 Proposed model for Y142 phosphorylation in the regulation of DNA damage repair versus apoptosis

γH2A.X leads to recruitment of MDC1 and the MRN complex for DNA damage repair; whereas di-γH2A.X (pSer139pY142) prevents MDC1 recruitment and instead promotes the recruitment of pro-apoptotic JNK-1 (Cook *et al.*, 2009).

1.3.6 Interaction with microcephalin protein (MCPH1)

Singh and colleagues (2012) sought to elucidate how mediator proteins interpret the mono- and di- phosphorylated forms of H2A.X and as such, looked at the role of the early DDR protein, microcephalin (MCPH1). The previous studies have indicated that pY142 is dephosphorylated gradually in response to DNA damage, in contrast to S139 which is phosphorylated rapidly in response to DSBs; therefore, they sought to identify a mediator protein capable of dual recognition of the overlapping states which could serve to recruit downstream mediator proteins.

MCPH1 has three BRCA C-terminal (BRCT) domains; the tandem C-terminal BRCT2 and BRCT3 domains have previously found to be necessary for irradiation-induced foci (IRIF) formation (Jeffers *et al.*, 2008) that colocalise with γH2A.X (Wood *et al.*, 2007).

They developed an antibody specific to di-phosphorylated H2A.X to examine its role in the DDR and to investigate whether MCPH1 is a binding partner. Their results suggest that following 10 Gy irradiation for 1-hr, that there is an initial phase of di-phosphorylated H2A.X formation, peaking at 1-hr post-irradiation, which is followed by a rapid decline (Figure 1-9). They also observed that following 10 Gy of irradiation, a Y142 mutant showed the initial γH2A.X formation following DNA damage, however this rapidly reduced to undetectable levels. This supports the previous findings (Xiao *et al.*, 2009; Cook *et al.*, 2009) in which it was suggested that phosphorylation of Y142 is necessary to maintain γH2A.X formation; however, a Y142 mutant previously failed to interact with MDC1, required for foci expansion.

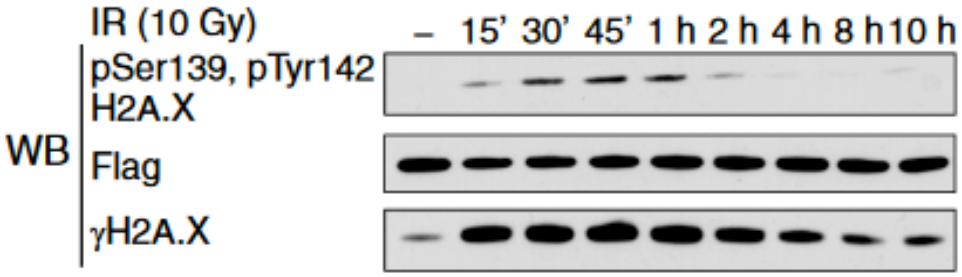

Figure 1-9 Kinetics of di-phosphorylated H2A.X after irradiation

H2A.X$^{-/-}$ MEF cells with Flag-SBP-tagged wild-type H2A.X were subjected to 10 Gy of irradiation for 1hr. Whole cell lysates were immunoblotted for γH2A.X and di-γH2A.X formation (Singh *et al.*, 2012).

Using pull-down assays, the group also determined that unlike MDC1, which only binds to γH2A.X, MCPH1 immunoprecipitated with both the mono- and di-phosphorylated forms of H2A.X, but not with pY142 (Singh et al., 2012).

1.3.6.1 Antibody validation

In order to validate their antibody, Singh and colleagues performed a dot blot with peptides corresponding to the different modified states of the C-terminal of H2A.X and probed them with the di-phosphorylated H2A.X antibody.

As can be seen at Figure 1-10, their antibody shows some cross-reactivity with both γH2A.X and pY142, and this may therefore influence the interpretation of the results found.

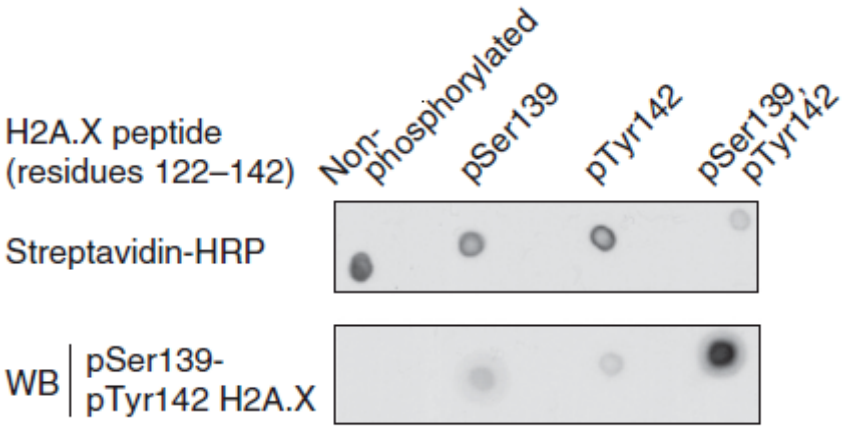

Figure 1-10 The di-phosphorylated H2A.X antibody has some cross-reactivity with γH2A.X (pS139) and pY142

Biotinylated peptides representing either unmodified, or mono- or di-phosphorylated H2A.X were spotted on nitrocellulose membrane and the membrane was then probed with pS139pY142 antibody, or streptavidin HRP (Singh *et al.*, 2012)

1.4 Eyes Absent (Eya) Tyrosine Phosphatases

1.4.1 Background

The Eyes Absent family of genes (*Eya1-4*) encode dual function Eya proteins that are both transcriptional coactivators and threonine/tyrosine phosphatases. These proteins are involved in embryonic organ development, fly eye development, the regulation of the innate immune response, cell motility, proliferation, and DNA damage repair. They are also implicated in promoting tumour cell migration and invasion (Okabe, Sano and Nagata, 2009; Cook *et al.*, 2009; Xiong, Dabbouseh and Rebay, 2009; Pandey *et al.*, 2010). Overexpression of Eya has been found in a number of human cancers and this elevated expression has been correlated with tumour aggressiveness and a poorer prognosis in some instances (Rebay, 2015).

1.4.2 Structure and activity

The transactivation and threonine phosphatase activity is contained within the poorly conserved, 200-300 residue amino-terminal domain; whereas the tyrosine phosphatase activity is contained within the conserved, 271-274 residue carboxy-terminal domain (Rayapureddi *et al.*, 2003).

In a study by Rayapureddi and colleagues, it was found that Eya3, of the bacterially generated Eya domains from mouse (Eya1-3), had the most potent phosphatase activity. Using phosphatase assays to identify the preferred substrates, they found that Eya3 showed no activity towards phosphoserine or phosphothreonine, but that it efficiently hydrolysed phosphotyrosine.

It could also dephosphorylate proteins in 293T cells in a dose-dependent and metal-dependent manner (Mg^{2+} or Mn^{2+}).

Their studies went on further to demonstrate that increased proliferation found in cells over-expressing Eya2 and Eya3 was not dependent on the tyrosine phosphatase activity. However, this activity of Eya was important for cell migration, invasion and transformation (Rayapureddi *et al.*, 2003).

1.4.3 Eya is phosphorylated by ATM/ATR kinases

Eya3 has previously been identified as a potential substrate for the DDR protein kinases ATM and ATR (Matsuoka *et al.*, 2007); Cook and colleagues found that Eya is phosphorylated at S219 in response to genotoxic stress (Cook *et al.*, 2009). Their studies found that a S219A mutant failed to interact with H2A.X or form nuclear foci after IR, unlike that of wild-type Eya (Figure 1-11 (A)). In further support of this, the inhibition of ATM/ATR using the PI(3)K inhibitor, caffeine, also resulted in a failure of Eya1 or Eya3 to interact with H2A.X following IR (Cook *et al.*, 2009) (Figure 1-11 (B)).

Furthermore, the depletion of Eya1 or Eya3 alone, using siRNA, was sufficient to prevent tyrosine dephosphorylation, and therefore suggested either a lack of compensatory activity between them or that they form a stable complex, with both components being required for enzymatic activity (Cook *et al.*, 2009).

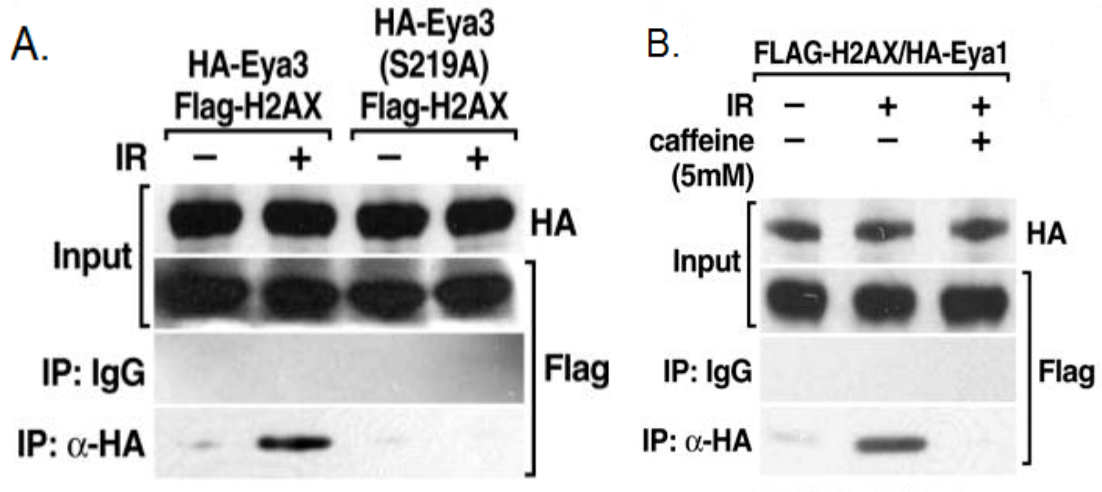

Figure 1-11 Eya phosphorylation at Ser-219, by ATM/ATR, is a requirement for H2A.X colocalisation

A. HA-Eya3 mutant (S219A) does not immunoprecipitate with Flag-H2A.X following 5 Gy of ionising radiation. **B.** HA-Eya1 does not immunoprecipitate with Flag-H2A.X in the presence of PI(3)K inhibitor, Caffeine, and following 5 Gy of ionising radiation (also seen for Eya3) (Cook *et al.*, 2009).

It is therefore speculated that upon DNA damage, Eya is regulated via phosphorylation at S219 by ATM/ATR, thus directing its tyrosine phosphatase activity towards pY142 and thereby facilitating the recruitment of DNA damage repair proteins. Furthermore, that through inhibition of Eya-mediated Y142 dephosphorylation, the formation of the subsequent di-phosphorylated H2A.X would promote the recruitment of pro-apoptotic proteins.

This has potential implications in cancer cells to promote apoptotic death; this current study therefore sought to elucidate whether the inhibition of Y142 dephosphorylation could be pharmaceutically mimicked with Eya inhibitors and whether this would result in an increase in cell death.

1.4.4 Eya Tyrosine Phosphatase Inhibitors

1.4.4.1 Eya active site

The Eya protein tyrosine phosphatases (PTPs) belong to the haloacid dehalogenase (HAD) type phosphotransferases (Tadjuidje *et al.*, 2012). They therefore represent an unconventional target for small molecule PTP inhibitors as, unlike all other known PTPs that utilise a cysteine residue for catalysis, these metallo-enzymes instead utilise aspartate as an acid catalyst (Rayapureddi *et al.*, 2005).

1.4.4.2 Inhibitor selection

An experimental screen of chemical inhibitors, by Tadjuidje and colleagues, found that the uricosuric agents Benzbromarone and Benzarone exhibited selectivity for, and were potent inhibitors of, the Eya tyrosine phosphatase activity. This was brought about by testing the hydrolytic activity of the catalytic domain of Eya3 (residues 223-510) against the substrate p-nitrophenylphosphate (pNPP), and further corroborated using a 10-amino acid phosphopeptide as an alternative substrate, one that represented pY142 at the C-terminus of γH2A.X (Figure 1-12).

An MTT assay conducted using a non-transformed mammary epithelial cell line (MCF10A) showed that the Eya inhibitors did not lead to any significant effect on cell proliferation (Tadjuidje *et al.*, 2012).

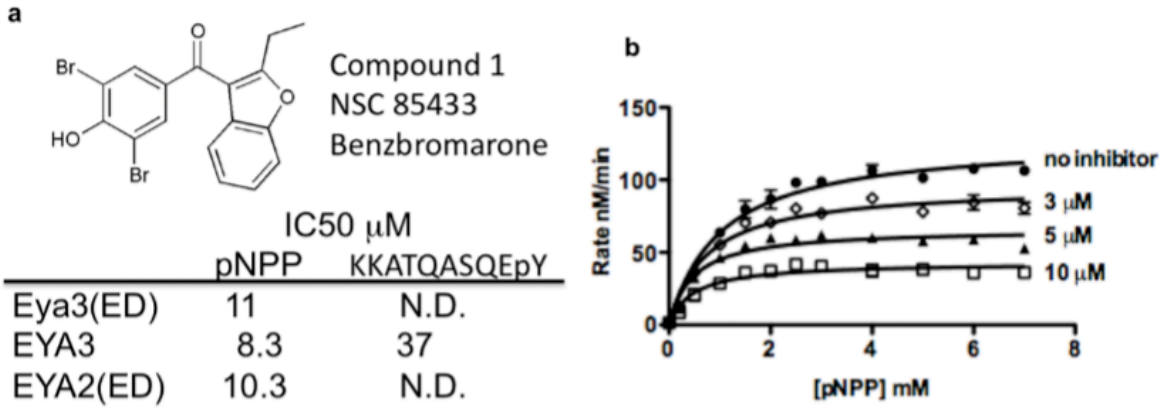

Figure 1-12 Benzbromarone is a potent inhibitor of Eya3

A. The IC50 values for Benzbromarone inhibition of Eya3 were calculated to be 8.3μM when using pNPP as a substrate and 37μM using a 10-amino acid phosphopeptide representing pY142 as a substrate. **B.** Increasing concentrations of substrate does not overcome Benzbromarone inhibition of Eya3, therefore it is an uncompetitive inhibitor.

1.5 Project outline

The study by Cook *et al*. put forward two key hypotheses:

1. That knockdown of Eya phosphatase activity led to an increase in apoptosis in cells, following damage by hypoxia or IR.
2. That the mechanism for this was an increase in the level of di-γH2A.X, which they proposed to be an epigenetic mark specifically associated with apoptosis.

The aim of this project was to therefore clarify the role of di-γH2A.X in the DDR, as well as in apoptosis. In addition, to test whether Benzbromarone - a pharmaceutical inhibitor of Eya - might be a useful adjuvant chemotherapeutic agent during treatment with DNA-damaging cancer drugs.

Co-operativity between Benzbromarone and the radiomimetic, chemotherapeutic agent, Bleomycin, was first investigated using the cell proliferation assay, MTT. The effect on apoptosis was then further assessed using an IncuCyte Live Cell Analysis System by detection of Annexin V and cleaved caspase-3/7.

Finally, immunochemical staining was performed to visualise the nuclear localisation patterns of both γH2A.X and di-γH2A.X, in cells undergoing both DNA repair and in apoptotic cells. For this project, I used a novel polyclonal antibody (supplied by Dr. Ellis) that was raised against di-phosphorylated H2A.X. Unlike the antibody used in previous published studies, the new antibody shows no cross-reactivity with either γH2A.X or pY142 (Figure 1-13).

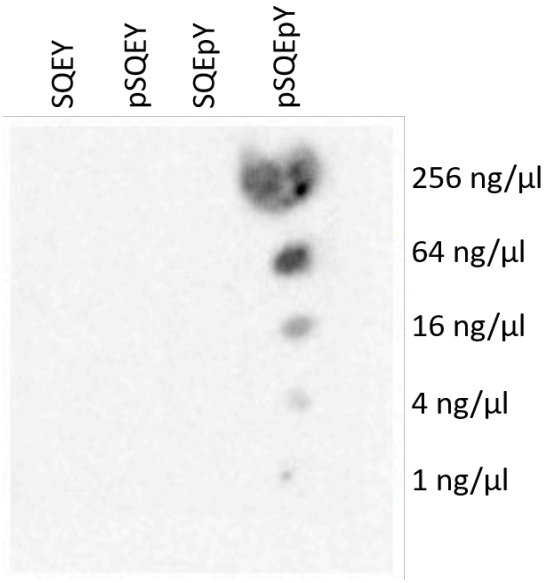

Figure 1-13 Validation of a novel polyclonal antibody raised against di-γH2A.X

Anti- di-γH2A.X antibody does not cross react with H2A.X or γH2A.X peptides. A dilution range of peptides, representing either unmodified H2A.X (SQEY), γH2A.X (pSQEY) or di-phosphorylated H2A.X (pSQEpY) were spotted on nitrocellulose membrane and the membrane was probed with the di-phosphorylated H2A.X antibody.

2 Materials and methods

2.1 Tissue Culture

Human Embryonic Kidney (HEK-293T) and Mouse Embryonic Fibroblast (MEF) cells were maintained in Dulbecco's Modified Eagle Medium (DMEM) with 1% L-Glutamine (ThermoFisher), supplemented with 10% foetal bovine serum (FBS) (ThermoFisher) and 1% penicillin/streptomycin (ThermoFisher). Cells were cultured at 37°C and 5% CO_2 and grown to confluency before splitting for passaging, which occurred every 4-days.

2.2 Nuclear protein extraction

HEK-293T cells were grown in T-175 tissue culture flasks, maintained in DMEM with 1% L-Glutamine, supplemented with 10% FBS and 1% penicillin/streptomycin at 37°C and 5% CO_2. Following treatment with 600IU (264μM) Bleomycin, cells were harvested by washing once with phosphate buffered saline (PBS) followed by the addition of 0.25% trypsin-EDTA. Cells were centrifuged at 1000 rpm for 5-mins, at 4°C, then the pellet washed twice in PBS. The cell pellets were washed again in ice cold hypotonic buffer containing 10mM Hepes (pH 7.9), 1.5mM $MgCl_2$, 10mM KCl, 1mM dithiothreitol (DTT), 50mM Benzbromarone, 0.5mM phenylmethylsulfonyl fluoride (PMSF), and a protease and phosphatase inhibitor cocktail (ThermoFisher), then centrifuged again at 1000 rpm for 5-mins, at 4°C.

Cells were then lysed by resuspending in the hypotonic buffer containing 0.1% NP-40 and incubation on ice for 30-mins, then mechanical shearing with a dounce homogeniser. The nuclei fraction was pelleted by centrifugation at 13,000 rpm for 10-mins, at 4°C, following which it was washed twice in PBS and then resuspended in a hypertonic buffer, for 15-mins on ice, containing 20mM Hepes (pH 7.9), 1.5mM $MgCl_2$, 420mM KCl, 25% Glycerol, 1mM DTT, 0.5mM PMSF, 50µM Benzbromarone, and a protease and phosphatase inhibitor cocktail (ThermoFisher). Samples were centrifuged at 13,000 rpm for 10-mins, at 4°C, to remove nuclear debris, and the supernatant containing nuclear proteins transferred to a fresh tube. The protein concentrations were quantified using a ND-1000 NanoDrop Spectrophotometer.

2.3 Acid extraction of histones

HEK-293T cells were seeded at a density of 1 x 10^6 cells in T-75 tissue culture flasks, maintained in DMEM with 1% L-Glutamine, supplemented with 10% FBS and 1% penicillin/streptomycin at 37°C and 5% CO_2. Cells were treated with/or without 8µM of Benzbromarone 24-hrs after seeding. 48-hrs post Benzbromarone treatment, cells were treated with/without 5µM of Bleomycin. At each specified time-point, the cells were trypsinised and collected in 50ml tubes. Cells were centrifuged at 300 rpm for 10-mins and the supernatant discarded; the cell pellet was then washed with PBS and re-centrifuged at 300 rpm for 10-mins and the supernatant again discarded. The cell pellet was then re-suspended and incubated in 1ml of ice cold hypotonic lysis buffer, containing 10mM Tris–Cl (pH 8.0), 1mM

KCl, 1.5mM $MgCl_2$, 1mM DTT, and a protease and phosphatase inhibitor cocktail (ThermoFisher), for 1hr at 4°C on a spinning rotator. The intact nuclei were pelleted by centrifugation at 10,000 rpm for 10-mins, at 4°C. The supernatant was discarded, the nuclei re-suspended in 400µl of 0.2M sulphuric acid (H_2SO_4) and incubated on a spinning rotator, overnight at 4°C. Samples were centrifuged at 13,000 rpm for 10-mins, at 4°C, to remove nuclear debris, and the supernatant containing histones transferred to a fresh tube; this was then neutralised by adding 4ul of 5M sodium hydroxide (NaOH) to 60ul of sample (in 0.2M H_2SO_4) - final pH-6.0, and protein concentrations quantified using a ND-1000 NanoDrop Spectrophotometer.

2.4 SDS-PAGE and Western blot analysis

The nuclear / histone extracts were prepared with either: 1) Bolt LDS sample buffer (ThermoFisher) with 10% 2-mercaptoethanol, heated at 70°C for 10-mins, followed by SDS-PAGE performed on either 10% or 15% handcast polyacrylamide gels with NuPage MOPS SDS running buffer containing 50mM MOPS, 50mM Tris Base, 0.1% SDS, 1mM EDTA, (pH 7.7); or 2) Novex Tris-Glycine SDS sample buffer (ThermoFisher) with 50mM DTT, heated at 70°C for 10-mins, followed by SDS-PAGE performed on a 16% pre-cast Tris-Glycine polyacrylamide gel (ThermoFisher) with Novex Tris-Glycine SDS running buffer containing 25mM Tris Base, 192mM Glycine, 0.1% SDS, (pH 8.3). Electrophoresis was performed at a constant voltage of 100v for 90-mins. After electrophoresis, proteins were transferred to a Polyvinylidene Difluoride (PVDF) membrane.

The PVDF membrane was then blocked in Tris-buffered saline (TBS) with 0.1% Tween-20 and 5% BSA for 60-mins, then incubated with either anti-pS139 primary antibody (1:5000, mouse monoclonal, PTM Biolabs) or anti-pS139pY142 (1:1000, rabbit polyclonal with two purifications, PTM Biolabs), overnight at 4°C. After incubation, the membrane was washed four times with TBS with 0.1% Tween-20 solution for 5-mins each, then incubated with HRP-conjugated secondary antibody (1:10,000), raised against the primary antibodies, for 1-hr at room temperature with agitation. Finally, the PVDF membrane was washed four times with TBS Tween-20 for 5-mins each, incubated with enhanced luminol-based detection (ECL) reagent and then exposed on a Syngene G:Box-fluorescence imager.

2.5 Cell viability / proliferation assays

96-well plates were either seeded directly, or prepared by incubating them in a 1mg/ml solution of Poly-D-Lysine, overnight at 4°C, followed by two washes with sterile distilled water and a single wash with 96% ethanol. HEK-293T and MEF cells were seeded at a density of 1 x 10^3 cells per well, in DMEM with 1% L-Glutamine, supplemented with 10% FBS and 1% penicillin/streptomycin at 37°C and 5% CO_2. Cells were treated with/without 8μM Benzbromarone and/or serial dilutions of Bleomycin (100μl total volume). These were incubated for 5-days, after which 1mM of 3-(4,5-dimethylthiazol-2-yl)-2,5-diphenyltetrazolium bromide (MTT) was added to each well (25μl of a 4.8mM stock) and incubated for 4-hrs.

The MTT assay involves the conversion of the water soluble MTT to an insoluble formazan. The formazan was then solubilised by addition of a sodium dodecyl sulphate (SDS) solution (pH 4.0) containing 20% SDS and 40% dimethylformamide (DMF) overnight, and the concentration determined by optical density at 570nm using a microplate absorbance reader.

2.6 Apoptosis assays (Annexin V / Cleaved Caspase 3/7)

96-well plates were prepared by incubating them in a 1mg/ml solution of Poly-D-Lysine, overnight at 4°C, followed by two washes with sterile distilled water and a single wash with 96% ethanol. HEK-293T cells were seeded at a density of 1 x 10^3 cells (100µl per well), in DMEM with 1% L-Glutamine, supplemented with 10% FBS and 1% penicillin/streptomycin, with/without 8µM of Benzbromarone and incubated at 37°C and 5% CO_2. 24-hrs later, media was removed from wells and replaced with fresh media in combination with 8µM Benzbromarone and/or dilutions of Bleomycin. Cells were incubated with either: 1) 1mM of $CaCl_2$ and IncuCyte Annexin V cyanine fluorescent dye (1:200, EssenBioScience), which emits a red fluorescent signal upon binding to exposed phosphatidylserine (PS); or 2) 5µM IncuCyte Caspase-3/7 Reagent (1:1000, EssenBioScience), which crosses the cell membrane and can be cleaved by activated caspase-3/7 to release a DNA-binding green fluorescent label. Cell growth and apoptosis was monitored using the IncuCyte Live-Cell Analysis System, capturing 4 images per well, every 2 to 4 hrs at 10x objective.

2.7 Immunofluorescence

Coverslips were prepared by incubating them in a 1mg/ml solution of Poly-D-Lysine, overnight at 4°C, followed by two washes with sterile distilled water and a single wash with 96% ethanol. Coverslips were place in a CELLBIND 6-well plate and HEK-293T cells were seeded at a density of 3 x 10^5 cells per well, 24-hrs prior to treatment with/without 8μM of Benzbromarone and incubated at 37°C and 5% CO_2. 24-hrs post-Benzbromarone treatment, when the cells had reached ~60% confluency, they were treated with/without 5μM of Bleomycin. At each specified time-point, the media was removed and cells washed twice with ice cold PBS. Cytoplasmic and loosely held nuclear proteins were first extracted by incubating the coverslips on ice in 200μl of ice cold cytoskeleton (CSK) buffer, containing 10mM PIPES, 300mM Sucrose, 100mM NaCl, 3mM $MgCl_2$, 1mM EDTA, with 0.1% (V/V) Triton X-100, for 1-min. Coverslips were then washed twice with 1ml of ice cold PBS, followed by extraction of the tightly held nuclear proteins by incubating the coverslips in CSK buffer with 0.5% (V/V) Triton X-100, on ice for 20-mins. Coverslips were washed three times with ice cold PBS and cells fixed by incubating them in 4% formaldehyde/PBS at 4°C for 30-mins. Following fixation, cells were quenched with 50mM ammonium chloride (NH_4Cl), for 15 mins at 4°C, to reduce potential auto-fluorescence, then washed three times with PBS and permeabilised with TBS/0.5% Triton X-100 for 10-mins. Coverslips were washed three times with TBS and then blocked in TBS with either 1) 0.1% Triton X-100 and 3% BSA, or 2) 0.1% Triton X-100 and 10% goat serum, at 22°C for 60-mins, to reduce potential background staining.

Coverslips were then incubated in primary antibody diluent (TBS with 0.1% Triton X-100 and 3% BSA), with anti-pS139 primary antibody (1:250, mouse monoclonal, PTM Biolabs), together with anti-pS139pY142 primary antibody (1:50, rabbit polyclonal with two purifications, PTM Biolabs), overnight at 4°C. Coverslips were then washed three times with TBS for 5 mins each and incubated in secondary antibody diluent (TBS with 0.1% Triton X-100 and 3% BSA) with fluorescein isothiocyanate (FITC) conjugated goat anti-rabbit (1:500; Abcam - ab6717) and either Alexa Fluor 647 donkey anti-mouse (1:500; ThermoFisher - A31571) or Texas Red goat anti-mouse (1:500; Abcam - ab6787) secondary antibodies, at room temperature for 1hr. Followed by a further three washes with TBS and then mounted onto a glass microscope slide using Vectashield mounting medium containing DAPI (4',6-diamidino-2-phenylindole hydrochloride). Imaging was conducted on either an Olympus BX-60 epifluorescence microscope equipped with a cooled CCD camera, with DAPI, FITC and Cy5 filters; or an or Olympus BX-61 epifluorescence microscope equipped with a cooled CCD camera, with DAPI, FITC and Texas Red filters.

3 Results

3.1 Validating antibodies

3.1.1 Dot blot

As previously shown in Figure 1-13, the novel di-γH2A.X antibody was first validated for its specificity by dot blot: a dilution range of peptides, representing either unmodified H2A.X (SQEY), γH2A.X (pSQEY) or di-phosphorylated H2A.X (pSQEpY) were spotted on nitrocellulose membrane and then probed with the anti-di-γH2A.X antibody.

Unlike the previously discussed anti- di-γH2A.X antibody used by Singh and colleagues (Figure 1-10), the results showed that it was specific for di-phosphorylated H2A.X (pSQEpY) and that there was no cross-reactivity with the peptides relating to unmodified H2A.X, or γH2A.X (Figure 3-1).

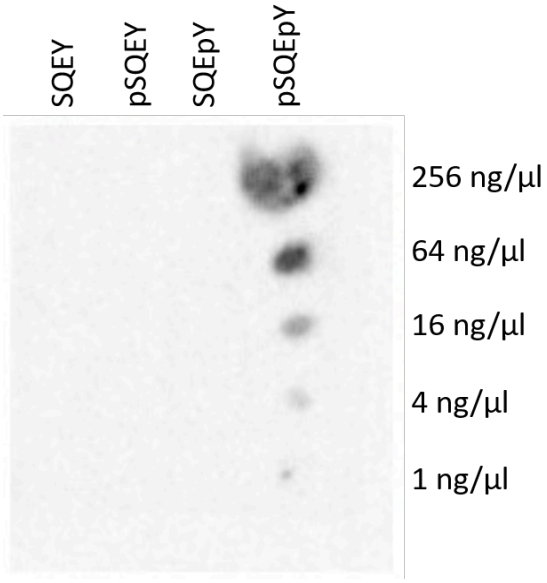

Figure 3-1 Validation of a novel polyclonal antibody raised against di-γH2A.X
Anti- di-γH2A.X antibody does not cross react with H2A.X or γH2A.X peptides. A dilution range of peptides, representing either unmodified H2A.X (SQEY), γH2A.X (pSQEY) or di-phosphorylated H2A.X (pSQEpY) were spotted on nitrocellulose membrane and the membrane was probed with the di-phosphorylated H2A.X antibody.

3.1.2 Nuclear protein extraction

To validate the antibody further using western blot analysis, nuclear extracts were prepared using a protocol developed for the extraction of nuclei from human tissue culture cells (Dignam, Lebovitz and Roeder, 1983). 293T cells were treated with 600IU (264μM) of Bleomycin, and nuclear proteins extracted between 1-hr and 4-days after continuous treatment. Both nuclear and cytosolic fractions were then separated using SDS-PAGE, transferred to a PVDF membrane and probed using the corresponding antibodies shown in Figure 3-2.

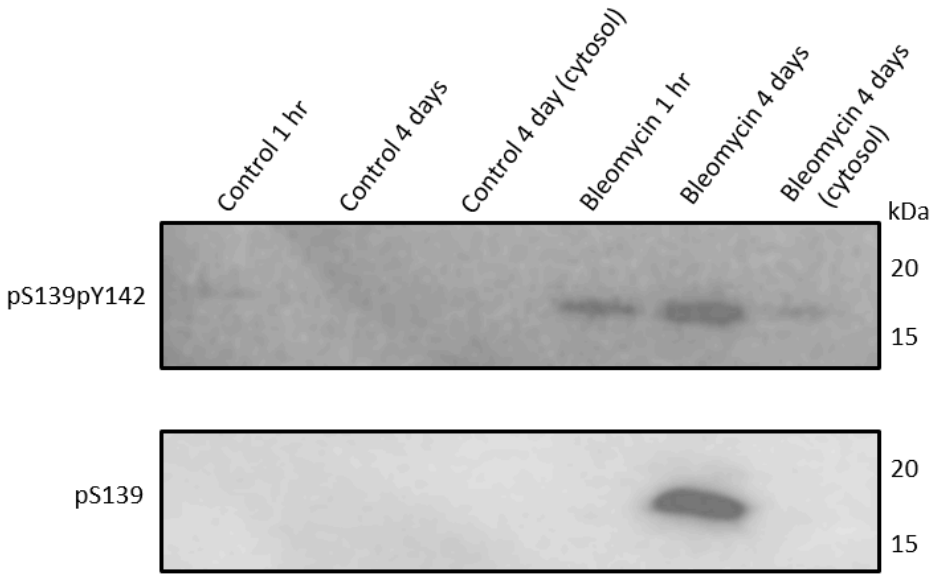

Figure 3-2 γH2A.X and di-γH2A.X expression following Bleomycin treatment

Di-γH2A.X was seen at the correct molecular weight of ~17kDa, as was γH2A.X; different expression levels are also seen for the two different antibodies, verifying that they are not cross-reacting. HEK293T were treated with 600IU of Bleomycin and nuclear proteins extracted. 38.7μg of both nuclear and cytosolic fractions were separated by SDS-PAGE using a 10% handcast gel, and probed with either anti-γH2A.X (pS139) or anti- di-γH2A.X (pS139pY142).

From this, it was possible to firstly determine that the di-γH2A.X antibody showed a band at the correct molecular weight for H2A.X (~17 kDa). Although separation of the nuclear fraction from the cytoplasmic fraction was not completely successful, shown from the band seen in the cytosolic fraction at 4-days probed with anti- di-γH2A.X, it did allow for visualisation of the different expression levels for the two different epigenetic states: strong induction of γH2A.X formation is seen at 4-day post-treatment. Although it is not seen at earlier time-points, as would be expected from the previously published results, earlier induction may not have been visible due to masking from the very strong signal at 4-days. In contrast, induction of di-γH2A.X is seen earlier, at 1-hr post-treatment. Similarly to γH2A.X, the strongest expression is at 4-day post-treatment, although with less total di-γH2A.X than γH2A.X. At 4-day post treatment with 264μM Bleomycin, the cells would be mostly apoptotic, as verified in later results.

3.1.3 Acid extraction of histones

To optimise extraction of the nuclear histones for better visualisation of di-γH2A.X, which is expressed in lower abundance than γH2A.X, an acid extraction protocol was next followed. Following hypotonic lysis of 293T cells treated with 5μM Bleomycin, histones were extracted using sulfuric acid (H_2SO_4) and neutralised using equivalent volumes of sodium hydroxide (NaOH). Histones were then separated using SDS-PAGE, transferred to a PVDF membrane and probed as before (Figure 3-3).

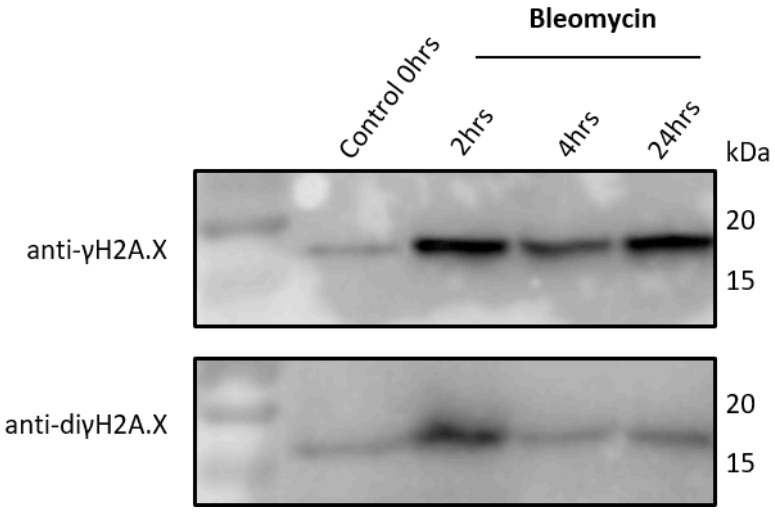

Figure 3-3 Acid extraction of histones show a different pattern of expression

Western blotting demonstrates that di-γH2A.X expression is different to that of γH2A.X. HEK293T cells were treated with 5μM of Bleomycin. Cells were harvested at the specified time points and histones extracted using H_2SO_4. 6.3μg of histone extracts were neutralised and separated by SDS-PAGE using a 15% handcast gel, probed with either anti-γH2A.X (1:5000) or anti- di-γH2A.X (1:1000) antibodies, then visualised using chemiluminescence.

Whereas the previous western blot focussed on histone modification expression at just 1-hr and 4-day post-Bleomycin treatment, this experiment observed earlier time-points; hence cells were harvested after 2-hrs, 4-hrs and 24-hrs of treatment. In addition, instead of using 264μM of Bleomycin as before, which would likely cause heavy DNA damage leading to rapid induction of apoptosis, 5μM of continuous Bleomycin treatment was used so that the mechanism of early attempts at DNA repair could be examined.

Once again, a different pattern of expression can be seen for γH2A.X and di-γH2A.X, further verifying the antibody specificities.

A strong induction of both γH2A.X and di-γH2A.X can be seen at 2-hrs post-treatment, more so with γH2A.X, which decreases at 4-hrs and increases again at 24-hrs. Di-γH2A.X expression decreases at 4-hrs and only increased again slightly at 24-hrs on this occasion. Interestingly, both γH2A.X and di-γH2A.X are seen in the control cells, suggesting that the HEK293T cells had some level of endogenous DNA damage, possibly from replicative stress.

3.1.4 Peptide competition assay

As a further verification step, a peptide competition assay was performed by western blot analysis. To do this, antibodies are incubated with an excess of peptide corresponding to the epitope that is recognised by the antibody; the antibody is therefore blocked and no longer available to bind the epitope that is present on the membrane.

293T cells were either pre-treated with 8μM Benzbromarone, 24-hrs prior to treatment with 5μM Bleomycin, or with 5μM Bleomycin alone. The cells were harvested at 30-mins, 1-hr, 4-hrs, and 24-hrs post-Bleomycin treatment. The 4-hr and 24-hr cells were rescued 2-hrs post-treatment by removal of Bleomycin and replacement of fresh media, either with or without 8μM Benzbromarone.

The cells were then subjected to hypotonic lysis to remove the cytoplasmic fraction, followed by acid extraction of the histones, using H_2SO_4. The extracts were neutralised as before, using NaOH, and separated by SDS-PAGE.

The proteins were transferred to a PVDF membrane and then probed with either anti-γH2A.X or anti- di-γH2A.X antibodies. In addition, the di-γH2A.X was pre-incubated overnight with either di-γH2A.X peptide or γH2A.X peptide, centrifuged at 12,000 rpm for 10-mins to pellet the immune complexes and then used to probe the PVDF membrane.

However, in order to successfully block the immunising antibody, an excess of corresponding peptide should be used, typically between 5-10 times weight/weight (w/w) to antibody. Unfortunately, on this occasion only 1 times w/w was used and therefore was unlikely to completely block the anti- di-γH2A.X antibody. This is reflected in the results shown at Figure 3-4, whereby pre-incubation of di-γH2A.X antibody with di-γH2A.X peptide fails to completely block the signal (Figure 3-4 (D)). Nevertheless, the signal is reduced in comparison to either di-γH2A.X antibody on its own, or di-γH2A.X pre-incubated with γH2A.X peptide (Figure 3-4 (D) as compared to Figure 3-4 (A) and (C) respectively).

Strong induction of γH2A.X is seen at 24-hrs post-Bleomycin treatment (Figure 3-4 (B)). Interestingly, on the three membranes probed with anti- di-γH2A.X antibody, two distinct bands for di-γH2A.X were evident: the expected ~17 kDa, as well as a smaller band at ~12 kDa. This cannot be explained at this time and so requires further investigation. The co-operativity between Bleomycin and Benzbromarone will be discussed in the next section.

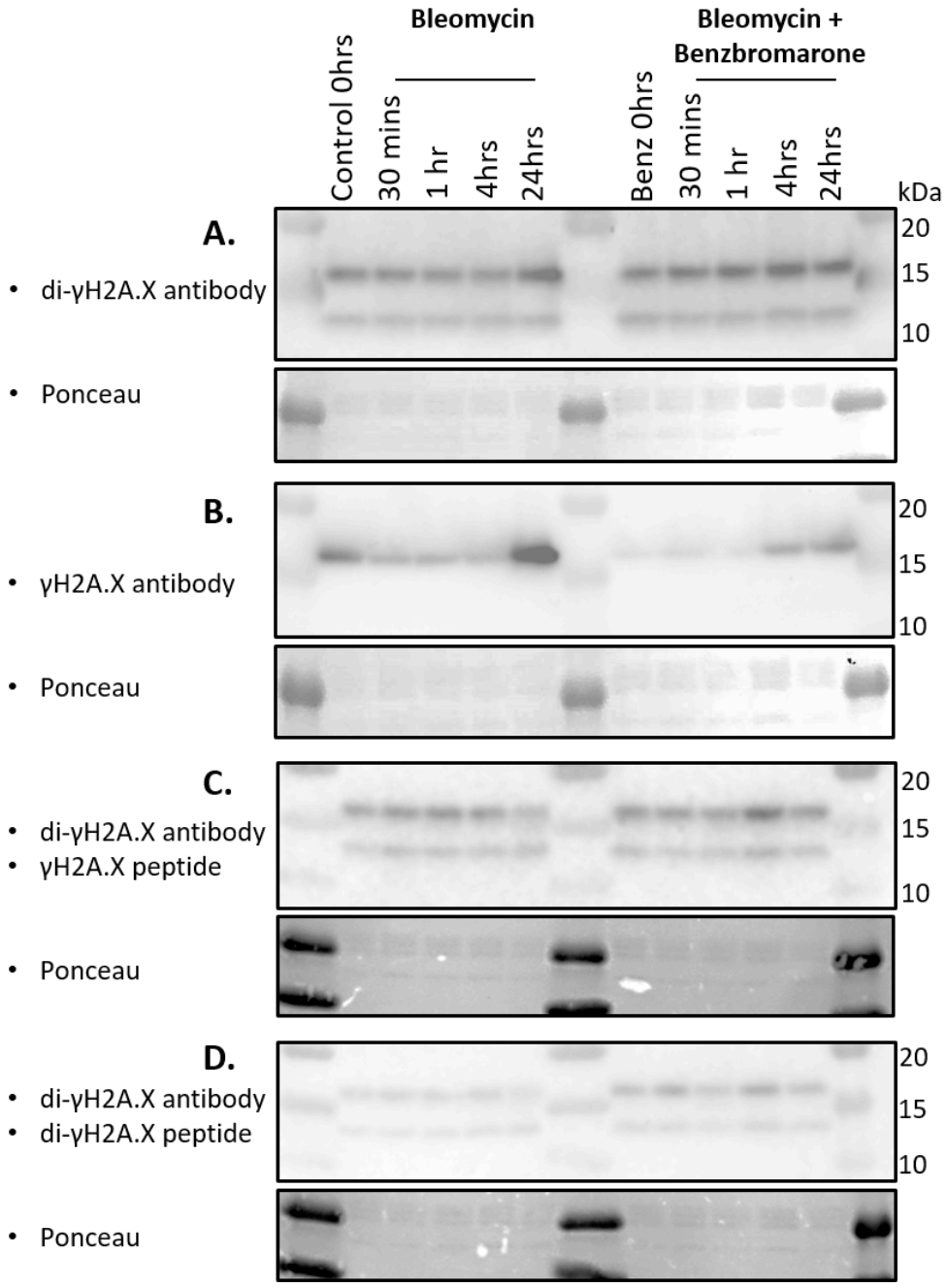

Figure 3-4 Antibody specificity analysed by a peptide competition assay on histone extracts
Peptide competition assay shows that di-γH2A.X peptide, but not γH2A.X peptide, is competitive for anti- di-γH2A.X antibody **(A-B)** HEK293T cells were treated with 5μM Bleomycin with/without 8μM Benzbromarone 24-hrs previously. 3μg of H_2SO_4 extracted histones were separated by SDS-PAGE, using a 16% pre-cast gel and probed with anti-γH2A.X (1:5000) or anti- di-γH2A.X (1:1000) antibody. **(C)** 7.2μg anti- di-γH2A.X antibody was first incubated with 7.2μg of γH2A.X peptide. **(D)** 7.2μg anti- di-γH2A.X antibody was first incubated with 7.2μg of di-γH2A.X peptide. Ponceau staining of histone extracts shown as a loading control.

3.2 Co-operativity between Bleomycin and Benzbromarone

3.2.1 Western blot results

To assess any co-operativity between Bleomycin and the Eya inhibitor, Benzbromarone, the expression levels of γH2A.X and di-γH2A.X were first compared by western blot analysis as shown previously.

The western blot at Figure 3-5 is an extended version of that already shown at Figure 3-3. From this, it is apparent that induction of γH2A.X is strong at 2-hrs post-Bleomycin treatment; this then reduces at 4-hrs post-treatment and increases again at 24-hrs. Although not a significant difference to that seen with pre-treatment of Benzbromarone prior to Bleomycin treatment, it does appear that inhibition of Eya by Benzbromarone causes slight reduction in γH2A.X levels at 2-hrs and 4-hrs post-Bleomycin treatment.

This same reduction in γH2A.X expression when pre-treated first with Benzbromarone was, however, seen more apparently at 30-mins and 1-hr in Figure 3-4 (B), with a clearly visible reduction in γH2A.X at these time-points. In this case, cells had been pre-treated with 8μM of Benzbromarone, 24-hrs before treatment with 5μM of Bleomycin. A recovery of γH2A.X levels is seen by 4-hrs post-treatment, yet by 24-hrs post-treatment, γH2A.X levels are significantly less to those that were not first pre-treated with Benzbromarone. In addition, di-γH2A.X levels appear to increase with pre-treated of Benzbromarone (Figure 3-4 (A)).

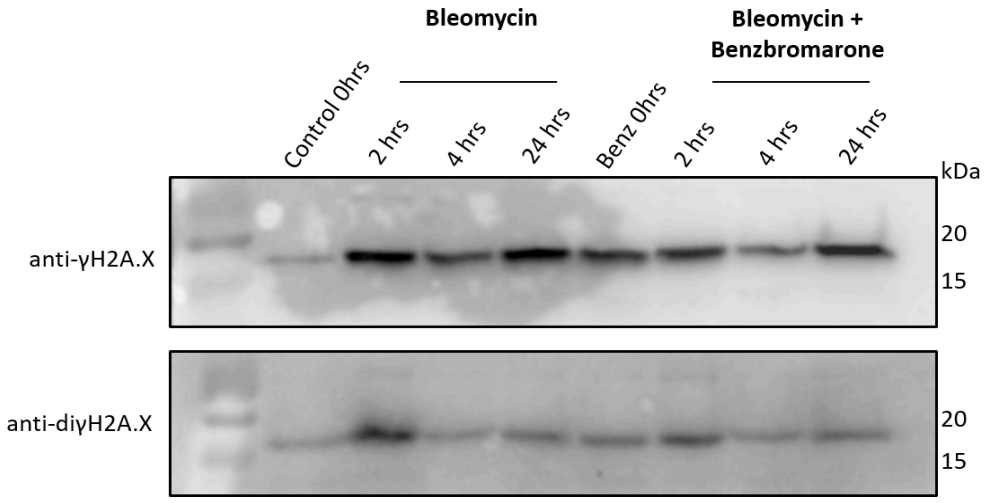

Figure 3-5 Western blot shows slight co-operativity between Bleomycin and Benzbromarone
Pre-treatment with Benzbromarone before Bleomycin causes slight reduction in γH2A.X expression. HEK293T cells were treated with 8μM of Benzbromarone, 48hrs prior to treatment with 5μM of Bleomycin. Cells were harvested at the specified time points and histones extracted using H_2SO_4. 6.3μg of histone extracts were neutralised and separated by SDS-PAGE, using a 15% handcast gel, probed with either anti-γH2A.X (1:250) or anti- di-γH2A.X (1:50) antibodies, then visualised using chemiluminescence.

3.2.2 Cell viability assays

3.2.2.1 MTT assays

To test the hypothesis of Cook and colleagues, in that inhibition of the removal of pY142 by the Eya phosphatase drives a molecular switch from DNA damage repair to apoptosis, pharmaceutical inhibition of Eya with Benzbromarone was used to assess the effect on cell viability. To do this, firstly the colorimetric tetrazolium salt assay, 3-(4,5-dimethyl-2-thiazolyl)-2,5-diphenyl-2H-tetrazolium-bromide (MTT) was used: this provides a measurement of metabolically active cells through the conversion of MTT to a purple coloured fomazan, the absorbance of which can then be read on a spectrophotometer.

As Eya phosphatase is known to have many cellular functions, we wanted to first determine the maximum concentration of inhibitor that would that have no independent effect on cell viability and therefore more likely that any co-operativity was a result of the proposed mechanism. An MTT assay was performed on both 293T and MEF cells, with triplicate technical repeats (Figure 3-6): from this it could be seen that there was ~100% cell viability at ~10μM (in comparison to control cells). As a result, 8μM of Benzbromarone was chosen for subsequent assays. There was a sharp decline in viability seen between 10 - 200μM in both cell lines, with an IC50 of 28μM in 293T cells and 65μM in MEF cells.

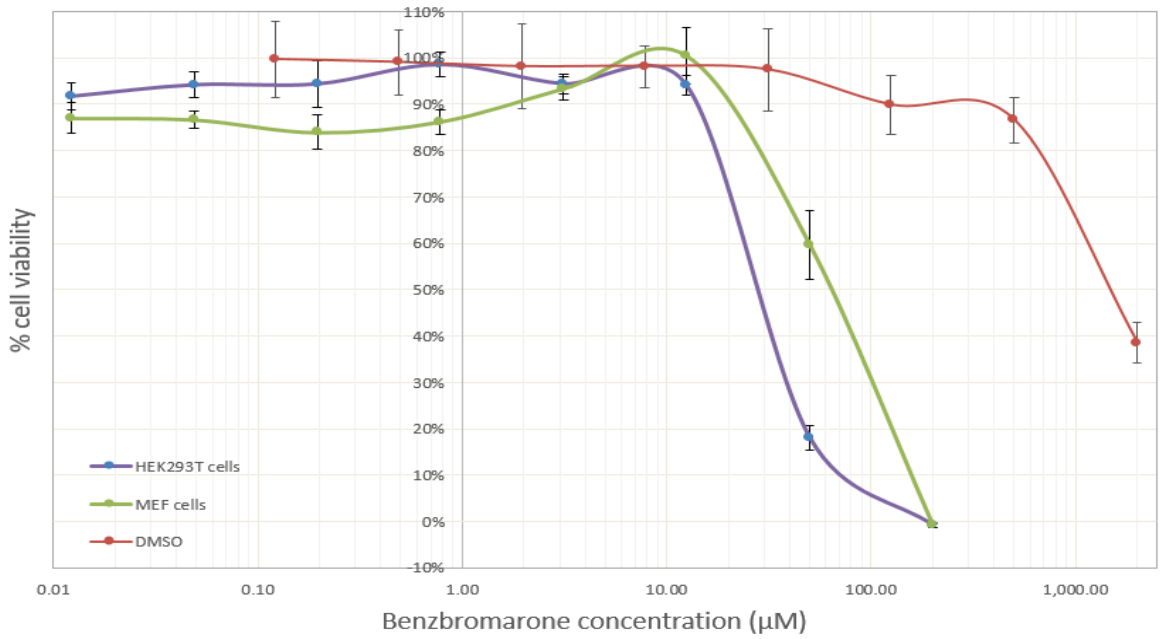

Figure 3-6 The effect of Benzbromarone and Dimethylsulfoxide on cell lines in vitro
Benzbromarone has an IC50 of 28μM in HEK293T cells and 65μM in MEF cells; Dimethylsulfoxide (DMSO) has no effect at this concentration of Benzbromarone in MEF cells. HEK293T and MEF cells were seeded in a 96-well plate and incubated with a serial dilution of either Benzbromarone; MEF cells were treated with an equivalent quantity of DMSO. After 5-days, MTT was added and the OD read at 570nm. Cell viability was calculated as a percentage of the untreated cells and each data point is an average of the triplicate repeats. Error bars based on standard deviation (SD).

As Benzbromarone is solubilised in dimethylsulfoxide (DMSO), equivalent dilutions of DMSO were used as a vehicle-only control in MEF cells (Figure 3-6): This shows a small decline in cell viability between 0.1 - 0.5% DMSO (equivalent to 125 - 500μM Benzbromarone) and a 60% decrease in cell viability at 2% total DMSO, which is equivalent to that which would be in 2mM Benzbromarone. Therefore, the decline in cell viability seen at greater than 10μM of Benzbromarone is not attributable to the effects of DMSO, other than possibly a small contribution at the maximum concentration of Benzbromarone.

MTT assays were then performed in both 293T and MEF cells, using 20μM Bleomycin as a starting concentration, with 4-fold serial dilutions and triplicate technical repeats. In addition, to determine if pre-treatment with Benzbromarone would increase the co-operativity with Bleomycin, by enabling uptake and inhibition of the Eya phosphatase prior to DNA damage by Bleomycin, cells were either pre-treated with Benzbromarone 24-hrs before or at the same as Bleomycin.

Each data point in Figure 3-7 is an average of each triplicate repeat: this MTT assay shows no co-operativity between Bleomycin and 8μM Benzbromarone. Unexpectedly however, a slight increase in viability is seen in MEF cells treated with Benzbromarone, which was seen in biological repeats and is of yet unexplained. The IC50 of Bleomycin in 293T cells was found to be 0.08μM, whereas MEF cells have slightly higher tolerance with an IC50 of 0.5μM.

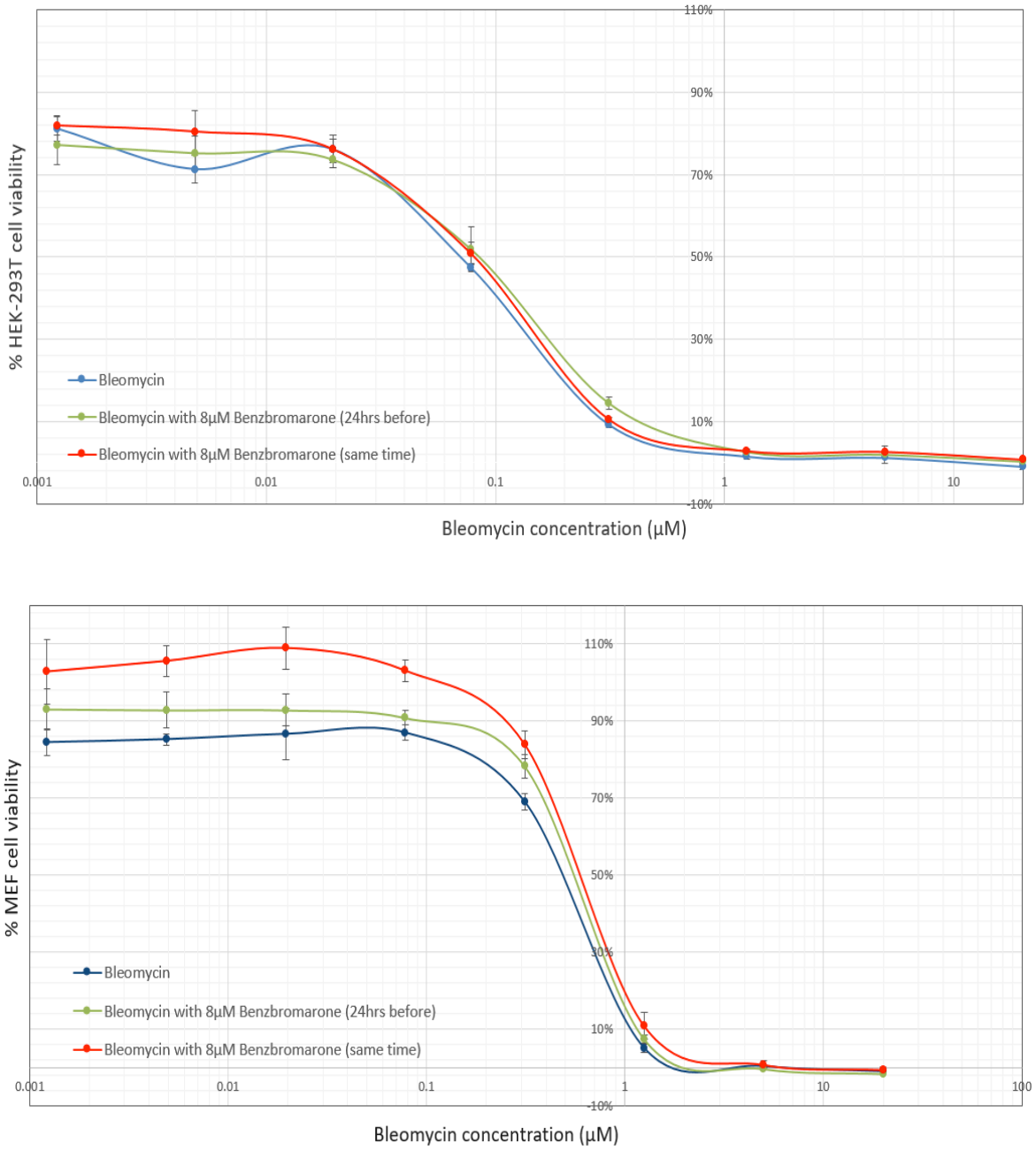

Figure 3-7 Cell viability assays (MTT) show no cooperativity between Bleomycin and 8μM of Benzbromarone

Co-treatment with Benzbromarone does not decrease the final percentage of viable cells. The IC50 of Bleomycin is 0.08μM in 293T cells and 0.5μM in MEF cells. HEK-293T cells (top) and MEF cells (bottom) were seeded in 96-well plates and incubated with 8μM of Benzbromarone either 24hrs before or at the same time as a serial dilution of Bleomycin. After 5-days, MTT was added and the OD read at 570nm. Cell viability was calculated as a percentage of the untreated cells. Error bars based on SD of triplicate repeats.

For subsequent MTT assays, 293T cells were instead treated with a pulse treatment of Bleomycin, which was removed after 2-hrs and replaced with fresh media with/without 8μM of Benzbromarone. The 96-well plate was first treated with Poly-D-Lysine, therefore the effect this may have on cell proliferation was measured (Figure 6-1 – Supplementary data). Cells were then either pre-treated with 8μM Benzbromarone 24-hrs before, at the same time, or 2-hrs after treatment with Bleomycin. The results seen indicate that again, there was no effect on cell viability by using a pulse treatment of Bleomycin, or by varying the timing of Benzbromarone administration. A pulse treatment of Bleomycin increased the IC50 to 0.65μM in 293T cells, compared to 0.08μM with continuous exposure.

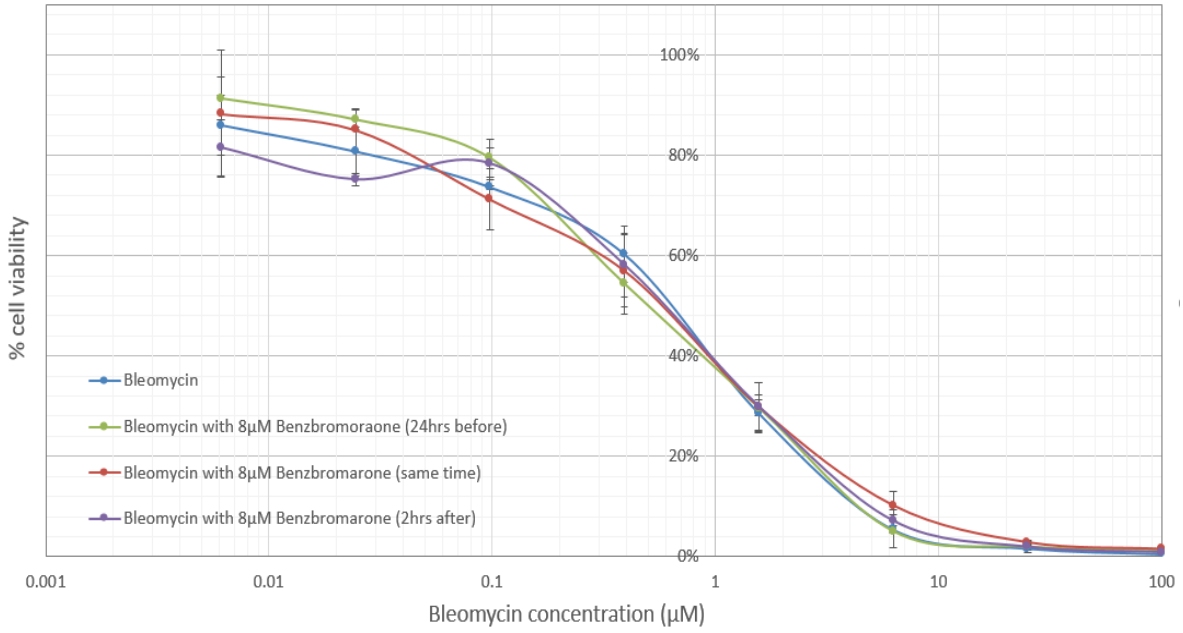

Figure 3-8 MTT assay shows no cooperativity between Benzbromarone and a pulse treatment of Bleomycin

Varying the timing of Benzbromarone co-treatment does not decrease the final percentage of viable cells; IC50 of Bleomycin with recovery is 0.65μM. HEK-293T cells were seeded as before and incubated with 8μM of Benzbromarone either 24hrs before or at the same time as a serial dilution of Bleomycin. Media was changed after 2hrs and replaced with fresh media, with/without 8μM of Benzbromarone. After 5-days, MTT was added and the OD read at 570nm.

3.2.2.2 Annexin V

To evaluate the induction of Bleomycin-induced apoptosis in cell culture, 293T cells were seeded in quadruple technical repeats in Poly-D-Lysine treated 96-well plates, either with or without 8μM of Benzbromarone. 24-hrs later, media was removed from wells and replaced with fresh media in combination with 8μM Benzbromarone and/or serial dilutions of Bleomycin. In addition, cells were incubated with 1mM of $CaCl_2$ and IncuCyte Annexin V cyanine fluorescent dye, which emits a red fluorescent signal upon binding to exposed phosphatidylserine (PS); PS is a marker of apoptotic cells and is externalised and displayed on the cell surface as an “eat-me” signal to phagocytes.

Cell growth and apoptosis was then monitored using the IncuCyte Live-Cell Analysis System, capturing 4 images per well, every 3-hrs at 10x objective for 86-hrs. The detection of both fluorescent signal and phase confluency was analysed first as an average of the 4-images per time point. These were then calculated as a ratio of Annexin V signal to phase confluency for each repeat, then an average taken across the quadruple repeats; this was then plotted for each dilution of Bleomycin. Graphs for 6.25μM and 25μM of Bleomycin are shown at Figure 3-9, which are representative of all concentrations: 6.25μM of Bleomycin was found to induce apoptosis in 9.89 ± 0.18% of cells at 86-hrs, and in 15.62 ± 3.26% of cells at 25μM. No increase in apoptosis was seen by co-treating with 8μM of Benzbromarone, or in the Benzbromarone only control sample.

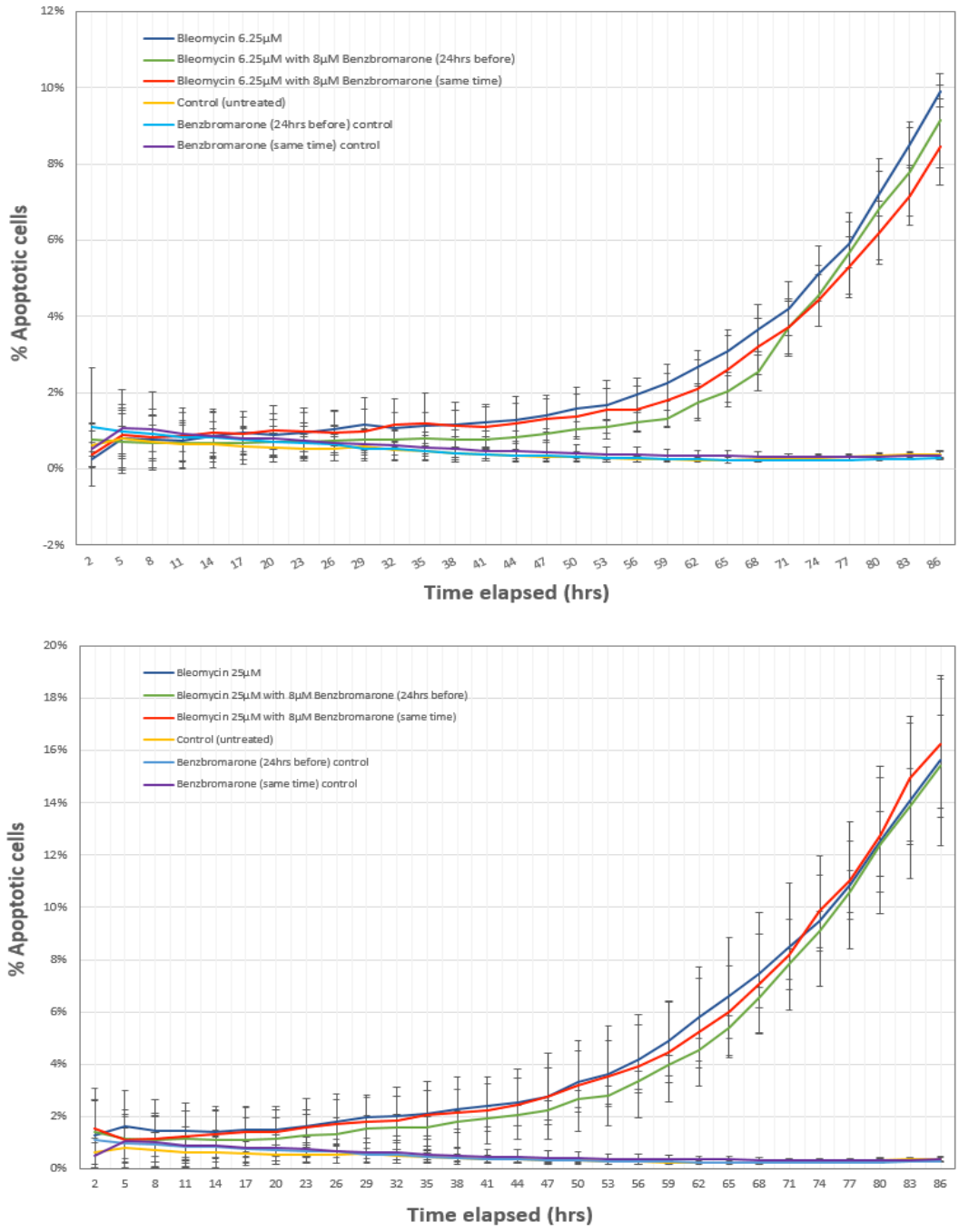

Figure 3-9 Apoptosis measured by Annexin V detection

There is no increase in apoptosis, as measure by Annexin V detection, by co-treating with Bleomycin and Benzbromarone. HEK293T cells were seeded in quadruple repeats in a 96-well plate, 1000 cells per well, with/without 8µM Benzbromarone. 24hrs later, cells were treated with a serial dilution of Bleomycin and incubated with Annexin V reagent in an IncuCyte Live-Cell Analysis System. Cell growth and apoptosis was monitored by capturing 4 images per well, every 3 hrs at 10x objective. Time elapsed represents time post-Bleomycin treatment. Error bars based on SD.

3.2.2.3 Cleaved Caspase 3/7

As a further evaluation of apoptosis induction, 293T cells were seeded and treated in the same manner as with Annexin V reagent. This time however, the cells were incubated with IncuCyte cleaved caspase-3/7 reagent; this reagent crosses the cell membrane where it can be cleaved by activated caspase-3/7 to release a DNA-binding green fluorescent label. Cell growth and apoptosis were monitored as before, capturing 4 images per well every 2-hrs, this time for 106-hrs.

Analysis was conducted in the same way as before (Figure 3-10). Shown first are 293T cells treated with either: 6.25μM of Bleomycin only; pre-treated with 8μM of Benzbromarone 24-hrs prior to treatment with 6.25μM Bleomycin; or with 8μM of Benzbromarone at the same time as 6.25μM Bleomycin. At 86-hrs post-Bleomycin treatment, the percentage of apoptosis induction was found to be 5.75 ± 0.37%; 5.78 ± 0.5%; and 5.13 ± 0.54% respectively. However, at 106-hrs, it was 14.87 ± 0.78%; 18.38 ± 4.23%; and 20.82 ± 1.29% respectively. The second graph shows 293T cells treated as above, but with 25μM of Bleomycin. At 86-hrs of post-Bleomycin treatment, the percentage of apoptosis induction was: 10.21 ± 3.46%; 12.78 ± 5.49%; and 20.95 ± 0.78% respectively. However, at 106-hrs, it was 21.04 ± 8.27%; 30.82 ± 13.09%; and 49.46 ± 5.01% respectively. Therefore, co-treatment of 25μM Bleomycin with 8μM Benzbromarone increased apoptosis more than 2-fold at 106-hrs. This was repeated with a pulse treatment of Bleomycin for 2-hrs (Figure 6-2- Supplementary data). A similar difference in apoptosis induction was found, although with less total apoptosis, as would be expected.

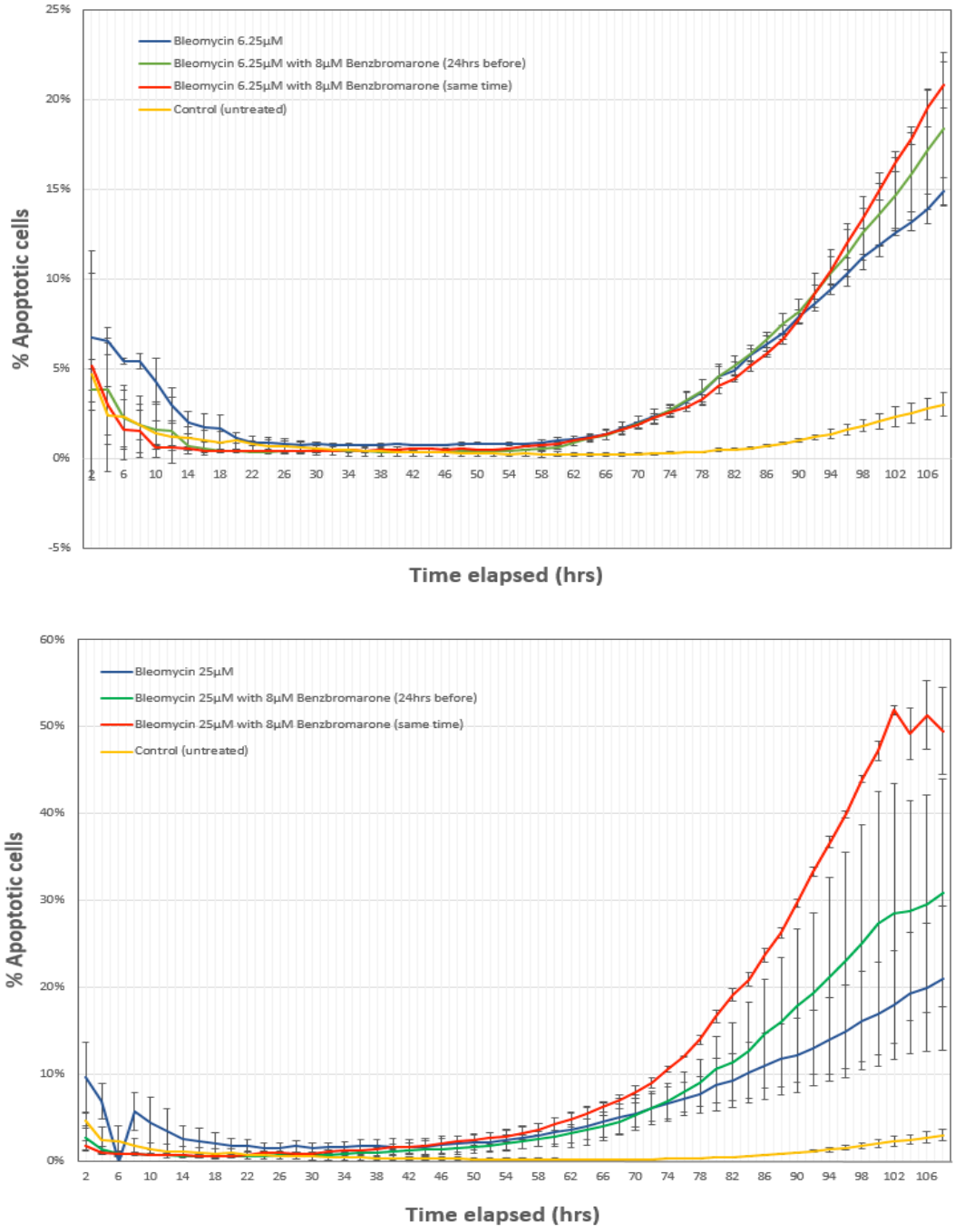

Figure 3-10 Apoptosis measured by cleaved Caspase 3/7 detection

Co-treatment of Bleomycin with 8µM of Benzbromarone increases apoptosis. HEK293T cells were seeded in quadruple repeats in a 96-well plate, 2000 cells per well, with/without 8µM Benzbromarone. 24hrs later, cells were treated with a serial dilution of Bleomycin and incubated with Caspase 3/7 reagent in an IncuCyte Live-Cell Analysis System for 106-hrs. Cell growth and apoptosis was monitored by capturing 4 images per well, every 2 hrs at 10x objective. Time elapsed represents time post-Bleomycin treatment. Error bars based on SD.

3.3 Immunofluorescence

To visualise the nuclear localisation patterns of γH2A.X and di-γH2A.X, 293T cells were grown on Poly-D-Lysine treated coverslips in a 6-well plate, until they reached ~60% confluency, at which point they were treated 5μM of Bleomycin for 2-hrs. The Bleomycin was removed and replaced with fresh media to allow a further 2-hr recovery period before extraction of the cytoplasmic and nuclear proteins using cytoskeleton (CSK) buffer. Following formaldehyde fixation, cells were quenched with ammonium chloride (NH_4Cl), permeabilised and immunofluorescence performed with anti-γH2A.X and anti- di-γH2A.X primary antibodies. Anti-γH2A.X was then labelled with AlexaFluor-conjugated secondary antibody; anti- di-γH2A.X was labelled with FITC-conjugated secondary antibody.

The results are seen at Figure 3-11. Figure A1 is a field view of untreated cells: of the 24 visible cells, 8 cells along the centre of the field show evidence of active DNA damage repair in the form of γH2A.X staining, ranging from 3-14 visible foci per cell. Consistent with western blot analysis, this again suggests some level of endogenous DNA damage in resting cells. Foci of di-γH2A.X are also visible in low abundance where γH2A.X is not visible, however the γH2A.X stained cells also stain highly for di-γH2A.X, demonstrating that di-γH2A.X foci increase as γ-H2A.X foci increase. Most intriguingly however, the majority of γ-H2A.X foci appear to be flanked by an adjacent di-γH2A.X focus that is in very close proximity to, but does not co-localise with γH2A.X. This is seen more clearly in the higher magnification of Cell 1 and Cell 2, at Figures A2 and A3 respectively.

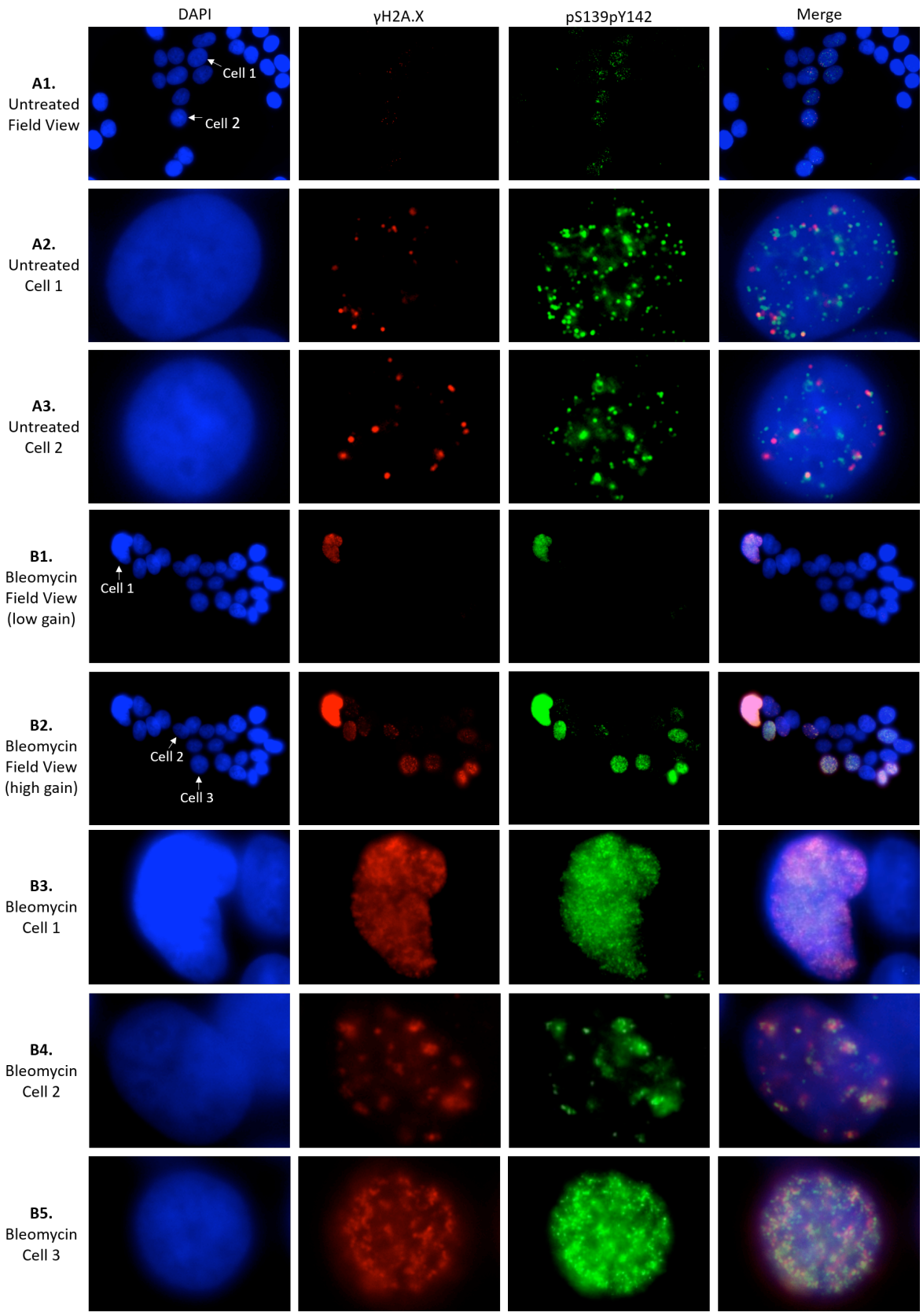
DAPI
γH2A.X
pS139pY142
Merge
A1. Untreated Field View
Cell 1
Cell 2
A2. Untreated Cell 1
A3. Untreated Cell 2
B1. Bleomycin Field View (low gain)
Cell 1
B2. Bleomycin Field View (high gain)
Cell 2
Cell 3
B3. Bleomycin Cell 1
B4. Bleomycin Cell 2
B5. Bleomycin Cell 3

Figure 3-11 Immunofluorescence shows adjacent localisation of γH2A.X and di-γH2A.X
Nuclei staining of HEK293T cells undergoing DNA damage repair shows that di-γH2A.X localises adjacent to γH2A.X. **(A1)** Untreated cells shown in a field view have visible signs of DNA repair foci **(A2-3)** Close-up view of Cell 1 and 2 from (A1) **(B1-B2)** Field view of cells 4-hr post-Bleomycin treatment, shown in low-gain and high-gain **(B3-B5)** Close-up view of Cells 1-3 from (B1-B2). Cells were grown on coverslips and either untreated, or treated with 5μM of Bleomycin for 2-hrs. Bleomycin was removed and media replaced for a further 2-hrs before extraction of the cytoplasmic and nuclear proteins using CSK buffer. Nuclei were fixed in PFA, quenched with NH_4Cl and permeabilised. Nuclei were blocked with 3% BSA and stained with anti-γH2A.X (1:250) and anti- di-γH2A.X (1:50) primary antibodies. Anti-γH2A.X labelled with AlexaFluor-conjugated secondary antibody (1:10,000); anti- di-γH2A.X labelled with FITC-conjugated secondary antibody (1:10,000); imaging on an Olympus BX-60 epifluorescence microscope with DAPI, FITC and Cy5 filters.

Figure B1 and B2 show the same field view of cells at 4-hr post-Bleomycin treatment: Figure B1 is at low gain and shows an apoptotic cell in the top left, stained highly with both γH2A.X and di-γH2A.X. The high gain of the same image, at Figure B2, reveals that in fact several of the cells are in various stages of DNA damage repair, ranging from small, distinct foci, to diffuse staining. Close-ups of cells 1-3 at Figures B3-B5 reveal the same pattern of staining seen previously, with di-γH2A.X foci seen adjacent to, but not co-localising with di-γH2A.X foci.

A biological repeat was conducted to evaluate whether this localisation pattern was consistent, the results of which are shown at Figure 3-12. This revealed the same pattern of adjacent staining of γH2A.X and di-γH2A.X in cells both undergoing DNA damage repair, as well an interspersed signal seen in apoptotic cells (Figure C1-C2). In addition to validating the authenticity of the previously seen results, a further intriguing finding was noticed in Figure A2, in which di-γH2A.X appears to be interdigitating with γH2A.X.

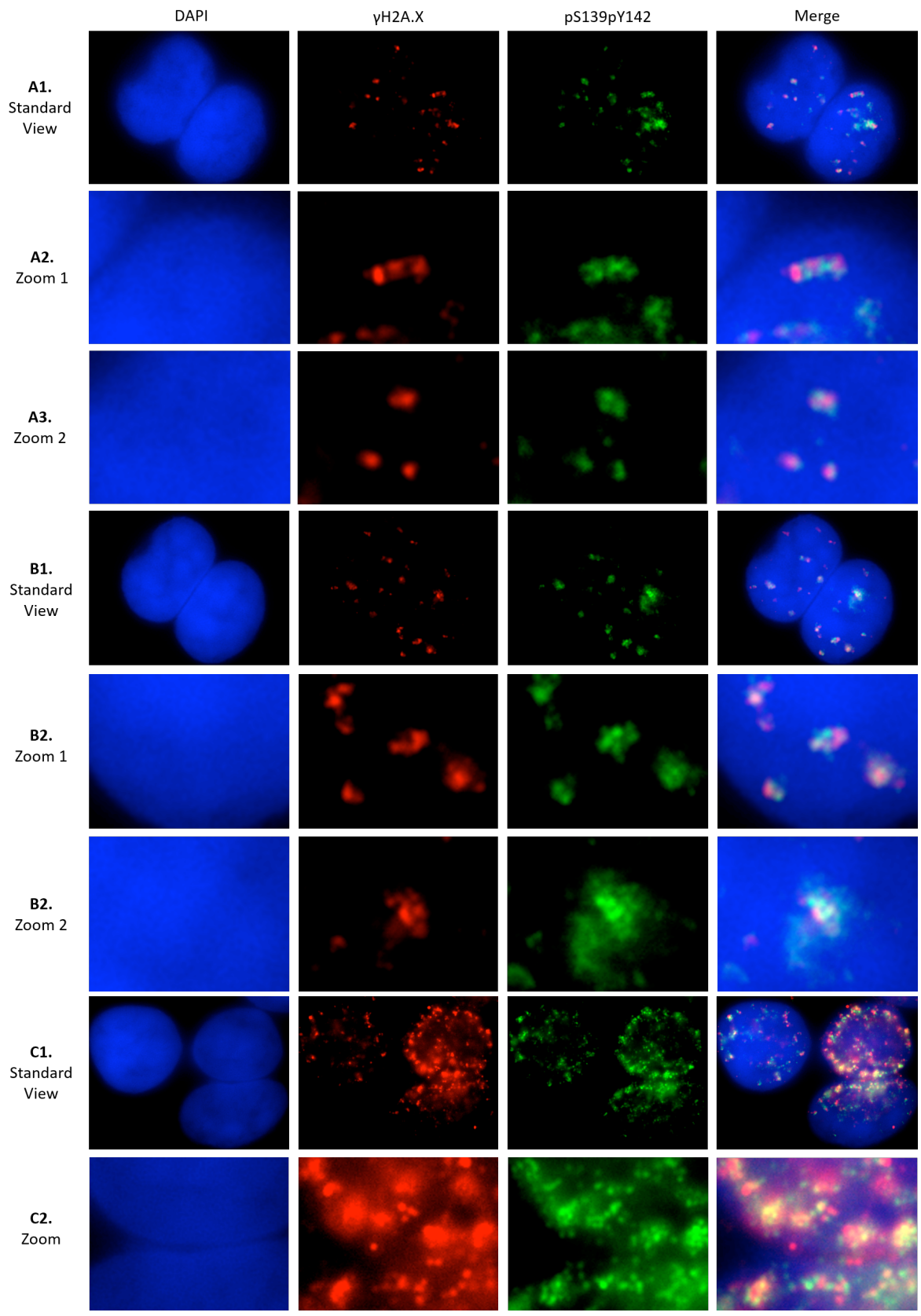
DAPI
γH2A.X
pS139pY142
Merge
A1. Standard View
A2. Zoom 1
A3. Zoom 2
B1. Standard View
B2. Zoom 1
B2. Zoom 2
C1. Standard View
C2. Zoom

Figure 3-12 Immunofluorescence biological repeats show same adjacent localisation of γH2A.X and di-γH2A.X

Nuclei staining of HEK293T cells show 1) cells undergoing DNA damage repair whereby di-γH2A.X localises in small, distinct foci adjacent to γH2A.X and 2) that there is interspersed and diffuse staining of γH2A.X and di-γH2A.X in apoptotic cells. **(A1)** Standard view of a pair of nuclei 4-hr post-Bleomycin treatment showing visible signs of DNA repair foci. **(A2-A3)** Close-up view of different regions of (A1), showing interdigitating and adjacent signals respectively. **(B1)** image of same pair of nuclei as in (A1) but taken in a different plane of focus and showing additional repair foci. (**B2-B3)** Close-up view of repair foci seen in (B1). **(C1)** Standard view of apoptotic cells showing the characteristic "apoptotic ring". **(C2)** Close-up view of (C1) showing interspersed signal of γH2A.X and di-γH2A.X. Cells were grown on coverslips and either left untreated, or treated with 5μM of Bleomycin for 2-hrs. Bleomycin was removed and replaced with fresh media for a further 2-hrs before extraction of the cytoplasmic and nuclear proteins using cytoskeleton (CSK) buffer. Nuclei were fixed in PFA, quenched with NH_4Cl and permeabilised. Nuclei were blocked with 10% goat serum and stained with anti-γH2A.X (1:250) and anti- di-γH2A.X (1:50) primary antibodies. Anti-γH2A.X labelled with Texas Red-conjugated secondary antibody (1:10,000); anti- di-γH2A.X labelled with FITC-conjugated secondary antibody (1:10,000). Imaging conducted on an Olympus BX-61 epifluorescence microscope equipped with a cooled CCD camera, with DAPI, FITC and Texas Red filters.

4 Discussion

4.1 Antibody validation

This study used a novel antibody raised against the di-phosphorylated form of H2A.X. The specificity of this was validated by dot blot and western blot analysis, peptide competition assays and immunochemical staining: dot blots showed that it does not cross-react with unphosphorylated H2A.X, or H2A.X phosphorylated at only S139 or Y142; western blot analysis revealed a band at the correct molecular weight with a pattern of induction that was distinct from γH2A.X; peptide competition assays showed a reduction in signal using a di-γH2A.X, but not γH2A.X peptide; and immunfluorescent staining of 293T cells show that it does not co-localise with γH2A.X and therefore has distinct epitope recognition.

4.2 Co-operativity of Benzbromarone

4.2.1 Cell viability assays

The first hypothesis of Cook *et al.* was that knockdown of Eya phosphatase activity led to an increase in apoptosis in 293T cells following DNA damage by 20-hrs of hypoxic conditions, or 5 Gy of ionising radiation. This project consequently sought to elucidate whether pharmaceutical inhibition of the Eya phosphatase could similarly lead to an increase in apoptosis following Bleomycin-induced DNA damage.

Eya 1-4 proteins are both transcriptional coactivators and tyrosine phosphatases, of which Eya3 has the most potent tyrosine phosphatase activity. Cell proliferation is not dependent on the tyrosine phosphatase activity, however, cell migration is (Rayapureddi *et al.*, 2003).

To test the hypothesis of Cook *et al.*, a concentration of Benzbromarone was selected that was found to have no independent effect on cell viability; thus any co-operativity could be attributed to the proposed mechanism, in that di-phosphorylated H2A.X leads to recruitment of pro-apoptotic JNK-1 with subsequent apoptosis.

A concentration of 8μM was subsequently selected and tested first by MTT assay. By incubating both 293T and MEF cells with a serial dilution of Bleomycin, either in the absence or presence of 8μM Benzbromarone, no effect on cell proliferation was observed. However, MTT assays afford a measurement of cell proliferation by determining the number of metabolically active cells at the end of the incubation period, but do not quantify apoptosis induction.

Nevertheless, this concentration of Benzbromarone was found to have some co-operativity in apoptosis assays conducted with an IncuCyte live-cell analysis system. Analysis was first performed by detection of an Annexin V cyanine fluorescent dye, which has high affinity for a marker of apoptosis, phosphatidylserine (PS).

Observations were first made over an 86-hr period, whereby no increase in PS detection was found by co-treating cells with Bleomycin and 8μM of Benzbromarone.

Yet when this was repeated using a further marker of apoptosis, cleaved caspase-3/7, a more than 2-fold increase in apoptosis was achieved after 106-hrs, by co-administration of 25μM of Bleomycin with 8μM of Benzbromarone. Rather than a difference in selectivity of the different apoptotic markers, the co-operativity found instead by cleaved caspase-3/7 detection is likely due to the extended analysis period: as at 86-hrs post-treatment, there was also little difference seen by caspase-3/7 detection. In support of this, studies by Varmark *et al.* (2009) assessed the long-term viability and proliferation of Bleomycin-treated human colon cancer (HCT116) cells: it was found that cell death occurred after an interphase delay of between 5–70 hrs. Interestingly, progression through mitosis following Bleomycin treatment was found to initiate a cell death response, linked to a significant increase in apoptosis.

In our study, 6.25μM of Bleomycin was found to induce apoptosis in 5.75 ± 0.37% at 86-hrs. This is also consistent with findings by Varmark *et al.* that 10μg/ml of Bleomycin (equivalent to 6.2μM) induced blocks in G_1 and G_2 progression, indicative of checkpoint activation at these two control points, but did not trigger high levels of cell death. This can therefore be considered a suitable concentration for the studies of early DNA damage repair mechanisms.

Since 8μM of Benzbromarone was shown to cause no independent increase in cell death, the increase found by co-administration could viably result from the mechanism proposed by Cook *et al.*, whereby inhibition of pY142 removal could lead to pro-apoptotic JNK-1 with subsequent apoptosis.

Unexpectedly, it was found that incubating cells with Benzbromarone at the same time as 25μM Bleomycin caused a larger increase in apoptosis than pre-treating cells with Benzbromarone 24-hrs prior to treatment with Bleomycin (49.46 ± 5.01% and 30.82 ± 13.09% respectively, at 106-hrs post-treatment). It was postulated that pre-treatment would maximise any cooperativity between Benzbromarone and Bleomycin by ensuring that Eya phosphatase was inhibited prior to DNA damage occurring. However, the half-life of Benzbromarone under cell culture conditions is unknown, and it may instead be that in the pre-treated sample, the Benzbromarone was degraded or metabolised prior to Bleomycin administration.

4.2.1.1 Cooperativity assays: limitations and future directions

4.2.1.1.1 Direct toxic effects of Benzbromarone

Benzbromarone is a uricosuric agent which acts by reducing the proximal tubular reabsorption of uric acid, however treatment with Benzbromarone or the non–halogenated Benzbromarone derivative, Benzarone, can be associated with hepatic injury through mitochondrial damage.

The mechanism of this has been determined in that they act as inhibitors of both the mitochondrial respiratory chain and β-oxidation, which leads to the uncoupling of oxidative phosphorylation.

In addition, they cause an increase in reactive oxygen species (ROS) and induce leakage of cytochrome c from the mitochondria, triggering apoptosis through caspase activation (Kaufmann *et al*., 2005). In a study of hepatotoxicity in rats, it was found that 20μM of Benzbromarone caused an 81% decrease in mitochondrial membrane potential, and a 54% decrease at the same concentration of Benzarone. Furthermore, 100μM of Benzbromarone or Benzarone increased ROS and induced leakage of cytochrome c from the mitochondria, and subsequent apoptosis (Kaufmann *et al.*, 2005). In flow cytometry studies using staining with Annexin V and propidium iodide, they showed that only 11% of rat hepatocytes that were exposed to 100μM of Benzbromarone were viable after 8-hr exposure.

In our studies, we did not investigate the direct toxicity effects of Benzbromarone, however we found that in our MTT assays, the IC50 of Benzbromarone was 28μM in 293T cells and 65μM in MEF cells, indicating that higher doses of Benzbromarone either directly kill these cell types or at least inhibit their proliferation. At present, we cannot tell whether these are direct toxicity effects of Benzbromarone or whether they are due to “on-target” effects of Benzbromarone in inhibiting Eya phosphatase activity (see next section).

4.2.1.1.2 IC50 of Benzbromarone

Whilst the IC50 for inhibition of Eya phosphatase by Benzbromarone has been found to be 8.1μM (7.4 - 9.3μM), this was measured for pNPP hydrolysis by Eya3 (Pandey *et al.*, 2013). Though using a phosphopeptide representing the last 10 amino acids of H2A.X, the IC50 of Benzbromarone inhibition of human Eya3 was instead found to be 37μM (Tadjuidje *et al.*, 2012). In our study, we deliberately chose the highest concentration of Benzbromarone that had no independent effect on cell viability, so that any co-operativity could be attributed to the mechanism proposed by Cook *et al.*

The chosen dose (8μM) is approximately the measured IC50 for inhibition of pNPP hydrolysis by Eya3, but is well below the measured IC50 of Benzbromarone when acting on H2A.X phosphopeptides, Thus, it is likely that only partial inhibition of Eya phosphotyrosine phosphatase activity had been achieved. It is potentially interesting that in the Benzbromarone-only arm of the MTT experiments, the IC50 of Benzbromarone was found to be 28μM in 293T cells and 65μM in MEF cells, i.e. a similar order of magnitude to the IC50 for inhibiting H2A.X phosphopeptide hydrolysis. It is possible that the growth inhibition seen in the MTT assays was in fact a consequence of “on-target” inhibition of Eya phosphatase activity, triggering apoptosis in response to endogenous double strand breaks. The difference in susceptibility between 293Ts and MEFs would then be attributable to differing levels of endogenous DNA damage – this could be tested in future experiments.

Additionally, to further assess whether Benzbromarone might still be a useful adjuvant chemotherapeutic agent during treatment with DNA-damaging cancer drugs, it would be of interest to repeat the cell viability assays, but using a higher concentration of Benzbromarone, at or around the IC50 for each cell type tested.

4.2.1.1.3 Alternative pharmacological methods of Eya inhibition

Benzbromarone was chosen for this study as it was found to be the most potent inhibitor of Eya phosphatase, with IC50s as shown above. However, it has a short plasma elimination half-life of approximately 3-hrs (Walter-Sack *et al.*, 1990; de Vries *et al.*, 1993), metabolised predominantly by cytochrome P450(CYP)2C9 in vitro (Uchida *et al.*, 2010). In contrast, the major metabolite of Benzbromarone, 6-hydroxybenzbromarone, has an increased half-life of approximately 30-hours (Uchida *et al.*, 2010). Although this is a less potent inhibitor of Eya, with an IC50 of 21.5μM (18.3– 25.3μM) measured by Eya3 mediated pNPP hydrolysis (Pandey *et al.*, 2013), it was also found to be a significantly more potent inhibitor of cell migration, tubulogenesis, and angiogenesis than Benzbromarone or its other derivates. Taken together, this may make 6-hydroxybenzbromarone an interesting candidate for future studies as a useful adjuvant chemotherapeutic agent.

Additionally, a novel benzofuran derivative, BL-038 (2-amino-3-(2,6-dichlorophenyl)-6-(4-methoxyphenyl)benzofuran-4-yl acetate), was recently evaluated for its effects in human chondrosarcoma cells.

This was found to cause apoptosis in two human chondrosarcoma cell lines, with an IC50 between 1.8 - 2.2μM by MTT assay, but did not affect the viability of normal primary chondrocytes. Apoptosis induction was found to be through increased ROS production, decreased mitochondrial membrane potential, downregulation of anti-apoptotic proteins (Bcl-2, Bcl-xL), and upregulation of pro-apoptotic protein (Bax, Bak and Bcl-2) (Liu *et al.*, 2016).

4.2.1.1.4 Alternative non-pharmacological methods of Eya inhibition

In view of the many functions of Eya, inhibition of which may result in independent initiation of apoptosis, an alternative to studying the involvement of pY142 phosphorylation in the decision between DNA-repair and apoptosis could be by selective inhibition of the phosphatase function of Eya, by mutation.

The nucleophilic acid in the first motif of the C-terminal Eya domain is the most commonly mutated to form a “phosphatase-dead” Eya, as shown in Figure 4-1 (Rebay, 2015). Though, there is debate about Eya’s phosphatase activity being intertwined with its transcriptional activity; for example, one study found that a phosphatase-dead Eya failed to recruit polymerase II (Pol II) and the coactivator CBP in a transcriptional reporter assay, leading to the conclusion that the phosphatase function was in fact necessary for the transcriptional activation of Six1-Dach (Li *et al.*, 2003).

However, a gene targeting approach to reducing Eya activity is further complicated by the presence of four paralogous genes that may complement each other in some cell types: it may be that several family members would need to be targeted simultaneously to achieve effective inhibition of Eya phosphatase activity.

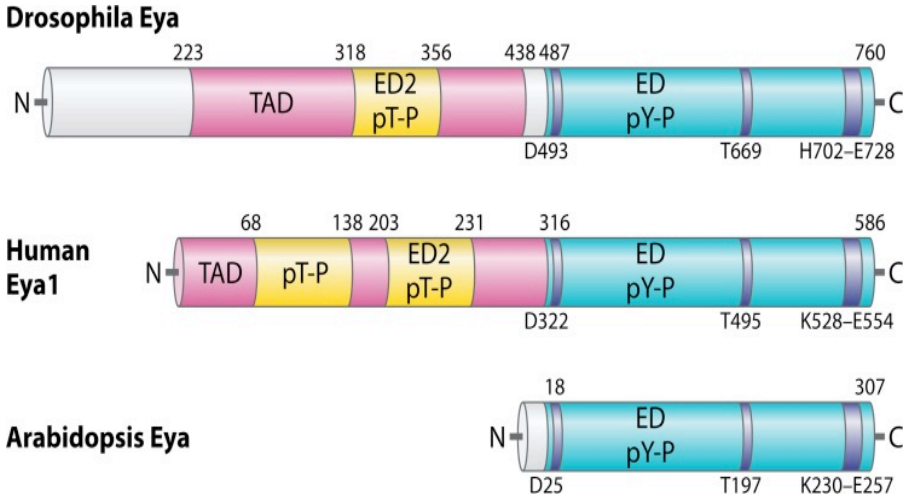

Figure 4-1 The functional domains of Eya family proteins

The phosphotyrosine (pY) domain of Eya are depicted as dark bars within the Eya domain (ED) at the C-terminal. The nucleophilic aspartic acid in the first motif is the most commonly mutated to form a “phosphatase-dead” Eya mutant (for example, D322 in human Eya1) (Rebay, 2015).

4.2.2 Western blot analysis

4.2.2.1 Intrinsic DNA damage in 293T cells

Both western blot analysis and immunofluorescent studies showed evidence of γH2A.X and equally di-γH2A.X, pre-existing in untreated control cells. This suggests a level of endogenous DNA damage in resting 293T cells, which could be a result of replicative stress or culture conditions. MEF cells were not used for western blot or immunofluorescence analysis, but it would be of interest to compare results between the two cell lines in future studies.

4.2.2.2 Kinetics of pS139 phosphorylation

Rapid and extensive phosphorylation on S139 (γH2A.X) occurs following DSB induction, followed by dephosphorylation (Rogakou *et al.*, 1998). The time-course for the induction and disappearance of γH2A.X foci was investigated in peripheral lymphocytes and found that unlike both IR treatment and UVB exposure, which cause maximal γH2A.X foci at 30-min post-exposure (Kinner *et al.*, 2008), Bleomycin induces a dose-dependent significant increase in γH2A.X foci at 1-hr post-treatment, with maximal induction seen at 2-hrs; followed by a progressive decrease at 3-hrs and 4-hrs (Scarpato *et al.*, 2013).

However, this depiction of γH2A.X kinetics is complicated by the findings of Ding *et al.* (2016). Shown in Figure 4-2, following X-ray irradiation of human peripheral blood lymphocytes, γH2A.X foci formation and pan-nuclear γH2A.X staining has two distinct kinetic patterns. The kinetics of γH2A.X foci formation was consistent with previous findings, with a peak induced rapidly after irradiation followed by an almost equally rapid decrease. In contrast, pan-nuclear γH2A.X staining increased steadily and was maintained, peaking at 24-hrs post-irradiation. Moreover, pan-nuclear γH2A.X staining was found to correspond with TUNEL staining, indicating that this staining is associated with apoptosis (Ding *et al.*, 2016).

In our study, the kinetics of pS139 induction was evaluated over either 24-hrs or 4-days post-Bleomycin treatment, with inconsistent findings.

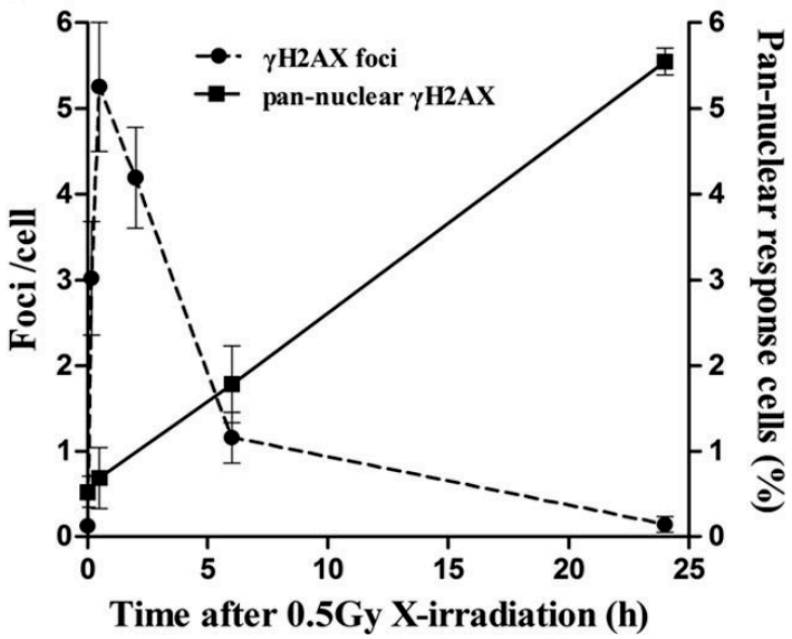

Figure 4-2 Kinetics of X-irradiation induced pan-nuclear γ-H2A.X vs γ-H2A.X foci formation
Resting human peripheral blood lymphocytes (HPBLs) were exposed to 0.5 Gy of X-ray irradiation. Foci of γH2A.X and pan-nuclear γH2A.X were quantified by counting 1000-5000 HPBLs at each time point. γH2A.X foci formation occurred rapidly, peaking shortly after irradiation, followed by a rapid decline. Whereas, pan-nuclear γH2A.X increased steadily post-irradiation, peaking at 24-hr post-exposure (Ding et al., 2016).

In this study, induction was investigated over 24-hrs, by acid extraction of histones at 2-hrs, 4-hrs and 24-hrs post-treatment with 5μM of Bleomycin (Figure 3-3): maximal pS139 induction was seen at 2-hrs, followed by a decline at 4-hrs then a further recovery to the maximal induction, at 24-hrs. Following the kinetics shown at Figure 4-2, this could be a result of extensive initial repair foci formation at 2-hrs, which decline significantly by 4-hrs; the strong signal reoccurring at 24-hrs is then likely to be a result of pan-nuclear γH2A.X in the apoptotic population.

However, in a further 24-hr study, also using acid extracted histones but at 30-mins, 1-hr, 4-hrs and 24-hrs post-treatment with 5μM of Bleomycin (Figure 3-4), strong induction was seen at 24-hrs but not before. Strangely, there was also higher levels of γH2A.X in the control cells than that seen in the early time-points of Bleomycin treatment.

During the 4-day study, 293T cells had been treated with 264μM of Bleomycin, likely to induce irreparable DNA damage and apoptosis in the entire population. Measurements were taken at just 1-hr and 4-days, and this time by nuclear protein extraction (Figure 3-2): strong induction was seen at 4-days, consistent with an entirely apoptotic population, yet no induction was seen at 1-hrs; though this earlier signal may have been masked by the very strong signal at 4-days.

Co-operativity between Bleomycin and Benzbromarone was seen, in that γH2A.X levels were decreased at 30-mins and 1-hr by treating cells with 8μM of Benzbromarone 24-hrs prior to 5μM of Bleomycin, and although some recovery was seen by 24-hrs, it was significantly less to that seen at 24-hrs with Bleomycin alone (Figure 3-4). In addition, there appeared to be an increase in di-γH2A.X through co-treatment with Benzbromarone. Thus, this could be a consequence of the conversion of pre-existing pY142 to di-γH2A.X following DNA damage, with inhibition of Eya abrogating its conversion to pS139.

4.2.2.3 Kinetics of pY142 phosphorylation and di-γH2A.X formation

Elucidating the kinetics of pY142 and di-γH2A.X phosphorylation has been somewhat hindered in past studies due to lack of specificity of antibodies.

Studies conducted by Xiao *et al.* suggest that Y142 is constitutively phosphorylated in MEF cells, and that following IR, pY142 is gradually dephosphorylated (Figure 1-5); Solier and colleagues also found that TRAIL-induced apoptosis caused a decrease in Y142 phosphorylation.

Singh *et al.* developed an antibody specific to di-phosphorylated H2A.X and their findings suggest that there is an initial phase of di-γH2A.X formation 1-hr post-irradiation, followed by a rapid decline (Figure 1-9). However, their study was only conducted over 10-hrs and their antibody cross-reacts with both pS139 and pY142.

Using the novel antibody raised against di-γH2A.X in this study, there was again inconsistent results. In some instances, there was strong induction at either 1-hr or 2-hrs post-Bleomycin treatment (Figure 3-3), followed by a rapid decline (as found by Singh *et al.*); in other instances, strongest induction was found at either 24-hrs (Figure 3-4) or 4-days (Figure 3-2). This may suggest however, that di-γH2A.X has roles in both early stages of the DDR, as well as later roles in apoptosis.

As mentioned previously, there also appeared to be some increase in di-γH2A.X formation through co-treatment of Bleomycin with Benzbromarone.

4.2.2.4 Kinetics of pY142 de-phosphorylation

A study conducted by Krishnan *et al.* (2009) looked further at the dephosphorylation of pY142 by Eya2 and Eya3 phosphatases, which corroborated findings that they have specificity for Y142 *in vitro.*

By testing synthetic peptides corresponding to either pS139, pY142 or pS139pY142 (di-γH2A.X) as substrates of Eya2 and Eya3, found that: both Eya2 and Eya3 were able to rapidly dephosphorylate pY142 (K_m 1.9μm and 1.8μm respectively) but not pS139 (K_m 80μm and 72μm), and could also dephosphorylate pS139pY142, yet with lower affinity than seen with pY142 (K_m 3.8μM and 3.5μM). Furthermore, in support of previous findings, siRNA inhibition of Eya lead to an increase in basal levels of pY142, as shown by western blot analysis, and inhibited dephosphorylation of pY142 following DNA damage.

However, the model proposed by Cook *et al.* suggests that siRNA inhibition of Eya leads to an increased conversion of pY142 to di-phosphorylated H2A.X, yet levels of pY142 did not decrease following IR and siRNA inhibition (Krishnan *et al.*, 2009). Though this may be as a consequence of their anti-pY142 antibody cross-reacting with the subsequent di-phosphorylated H2A.X (details of the antibody used were not provided).

4.3 Nuclear localisation of γH2A.X and di-γH2A.X

4.3.1 Immunochemical findings

The second hypothesis of Cook *et al.* is that Y142 is constitutively phosphorylated by WSTF at basal levels in undamaged cells, and gradually dephosphorylated by Eya following IR. Inhibition of Eya phosphatase thus leads to an increase in the level of di-γH2A.X, which they postulate to be an epigenetic mark specifically associated with apoptosis. This model was somewhat supported by Xiao *et al.* (Figure 1-5), in which pY142 decreased following IR, found by western blot analysis, though di-γH2A.X formation was not assessed. The decrease in pY142 found could be a consequence of either pY142 conversion to Y142, or to di-γH2A.X.

To visualise the nuclear localisation patterns of γH2A.X and di-γH2A.X during the DDR, immunofluorescence was performed on 293T cells after treatment with Bleomycin. Cells were visualised in various stages of the DDR, ranging from a few small, distinct γH2A.X foci in early repair, to diffuse staining and the characteristic “apoptotic ring” in heavily damaged, unrepairable cells. In contrast to the hypothesis of Cook *et al.*, di-γH2A.X foci were found to be localising with γH2A.X foci in early DNA repair, not just in apoptotic cells and increased at rates comparable vis-à-vis with γH2A.X. More specifically, the majority of γH2A.X foci appeared to be flanked by an adjacent di-γH2A.X focus and intriguingly, appeared to be interlocking in some cases. Apoptotic cells were found to have an interspersed signal of both γH2A.X and di-γH2A.X.

4.3.2 New model of repair focus maturation

As a result of the immunochemical studies, we propose a new model for the role of di-γH2A.X in the DDR (shown at Figure 4-3). We postulate that in support of previous findings, resting chromatin contains H2A.X that has basal levels of phosphorylated Y142 (Xiao *et al.*, 2009). Following DSB induction, H2A.X is phosphorylated at S139 by ATM/ATR kinases, forming γH2A.X (Pilch *et al.*, 2003) (Zhu *et al.*, 2011); this allows recruitment of MDC1 (Stewart *et al.*, 2003), which in turn recruits the MRN complex and in turn, additional ATM (You *et al.*, 2005). ATM subsequently phosphorylates further S139 residues on adjacent H2A.X, allowing the spread of γH2A.X signalling *in cis* along the chromosome, moving outwards from the break site. This spreads the γH2A.X signal until which point it reaches an H2A.X that is already phosphorylated on Y142.

Our new model suggests that at this stage, the phosphorylation of S139 on this H2A.X, already phosphorylated at Y142, thereby causes formation of di-γH2A.X. Since di-γH2A.X is unable to bind MDC1 (Cook *et al.*, 2009; Campbell, Edwards and Glover, 2010), thus we propose that instead of being a determining factor of an epigenetic switch from DNA repair, to apoptosis, that this instead prevents the perpetual spreading of γH2A.X, allowing the retention and accumulation of DDR proteins at the site of DSBs. The lower affinity removal of pY142 by Eya phosphatase then converts di-γH2A.X to γH2A.X, allowing recruitment of more MDC1/MRN complex/ATM. Consequently, this enables phosphorylation of surrounding H2A.X and the γH2A.X repair focus to enlarge as it matures.

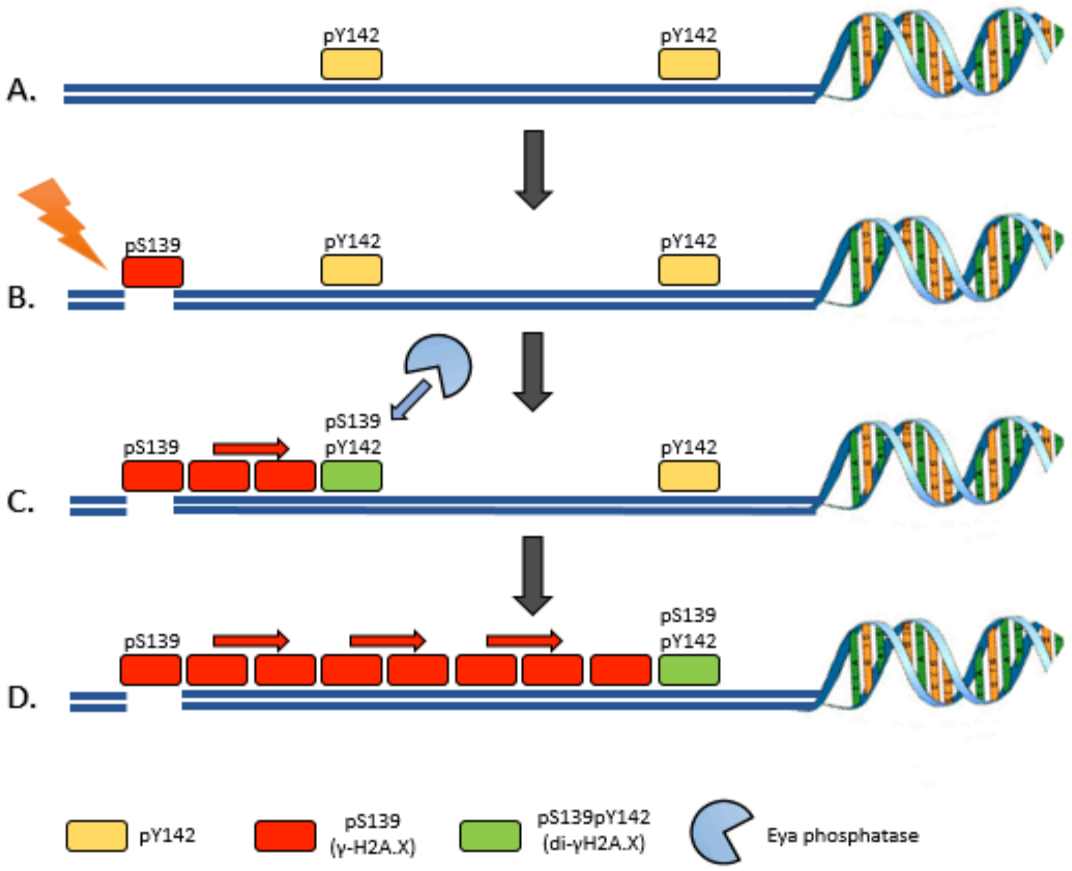

Figure 4-3 Proposed new model of the role of di-γH2A.X in the DDR

A. Resting chromatin contains H2A.X that has basal levels of phosphorylated Y142 (pY142) **B.** At sites of DSBs, ATM/ATR kinase phosphorylates S139 of H2A.X, forming γH2A.X; this allows recruitment of MDC1, which in turn recruits the MRN complex and more ATM; ATM phosphorylates further S139 residues on adjacent H2A.X, allowing the spread of γH2A.X signalling *in cis* along the chromosome, moving outwards from the break site **C**. The γH2A.X signal spreads until it reaches an H2A.X that is already phosphorylated on Y142; phosphorylation of S139 on this H2A.X causes formation of di-γH2A.X. Di-γH2A.X blocks MDC1 recruitment and prevents the signal spreading further until Eya phosphatase converts the di-γH2A.X to γH2A.X by removing pY142 **D.** During repair focus maturation, the removal of pY142 by Eya phosphatase allows γH2A.X to recruit more MDC1; MDC1/MRN complex/ATM enables phosphorylation of surrounding H2A.X; this enables the γH2A.X repair focus to enlarge as it matures.

Also interesting in this context are the findings of Xiao *et al*.: their western blot analysis showed that, in contrast to the increase in γH2A.X seen 1hr post-IR, which was sustained until 12hrs post-IR in wild-type cells, WSTF RNAi cells had initial formation of γH2A.X at 1hr post-IR, but that this was not maintained and had sharply decreased by 4hrs post-IR. This indicates that WSTF mediated phosphorylation of Y142 is necessary to maintain γH2A.X formation. Our model does not directly touch on this hypothesis, however our observation of adjacent localisation of mono- and di-γH2A.X domains may indicate that di-γH2A.X has some role in stabilising γH2A.X within chromatin.

While a lot of research has thus far been directed towards the assembly of γH2A.X foci, very little is known about how they are disassembled after repair: the role of pY142 and di-γH2A.X in this will be interesting to explore, e.g. via work in WSTF-null and Eya-null backgrounds.

4.3.3 Apoptosis and caspase activated DNAse (CAD)

Activation of DDR proteins occurs rapidly following IR induced DSBs, including auto- or trans-phosphorylation of ATM (pATM) at S1981 (Bakkenist and Kastan, 2003; So, Davis and Chen, 2009) and autophosphorylation of DNA-PK (pDNA-PK) at T2609 (Chan *et al.*, 2002). During the study of γH2A.X kinetics by Ding *et al.,* they noted that in addition to correlation of pan-nuclear γH2A.X with TUNEL staining, that both pATM and pDNA-PKs foci formation followed a very similar pattern to that of γH2A.X foci, indicative of their role in the DDR.

However, pan-staining of both pATM and pDNA-PK was found to follow a different kinetic pattern in that induction was slower than that of foci formation, peaking at 6-hrs post-irradiation and decreasing to zero by 24-hrs. Inhibitors of ATM and DNA-PK, p53 or pan-caspases all resulted in significantly less pan-nuclear γH2A.X, concluding that ATM and DNA-PK are therefore related to p53-dependent, caspase-3 dependent apoptosis induction, but are only activated at early stages. Solier *et al*. also found that the apoptotic ring colocalises with phosphorylated histone H2B (at serine-14), CHK2, ATM and DNA-PK (Solier *et al.*, 2012)..

Furthermore, caspase activated deoxyribonuclease (CAD) is normally sequestered in the cytoplasm as an inactive complex with its inhibitor ICAD, but is released by caspase-3 cleavage during apoptosis and is able to diffuse into the nucleus from outside-in, where it creates double strand breaks to initiate γH2A.X-dependent DNA degradation (Nagata *et al.*, 1998; Rogakou *et al.*, 2000; Lu *et al.*, 2006). It is therefore proposed that the “apoptotic ring” is formed first at the nuclear periphery as a consequence of the influx of CAD and subsequent H2A.X phosphorylation, with successive spread inwards leading to pan-nuclear γH2A.X.

Our immunofluorescence studies found evidence of both γH2A.X and di-γH2A.X in the apoptotic ring; whilst the mechanism of this has not been fully elucidated, it is plausible that upon apoptosis induction and influx of CAD, DSBs are formed that are phosphorylated at S139 on surrounding H2A.X by pDNA-PK/pATM; pre-existing pY142, present at the nuclear periphery, may then be rapidly converted to

di-γH2A.X through the phosphorylation of S139, resulting in the interspersed signal found. This rapid phosphorylation event thus may decrease the efficiency in which Eya phosphatase can dephosphorylate pY142, leading to a "blockade" in the recruitment of DDR proteins, and instead allow the recruitment of pro-apoptotic JNK-1, propagating the apoptotic response.

4.3.4 Limitations of immunofluorescence and future directions

4.3.4.1 3-D confocal imaging

A clearer depiction of γH2A.X and di-γH2A.X nuclear localisation patterns would be achieved via super-resolution imaging and/or 3-D imaging of chromatin, providing a higher resolution understanding of the nuclear architectural microenvironment.

4.3.4.2 Targeted systems for inducing DSBs

In addition to a comparative study using alternative means of DNA damage induction to determine if this model is consistent in other DSB repair mechanisms (i.e. γ-irradiation, hypoxia treatment, topoisomerase inhibition), of interest would be the use of a more targeted system to allow for temporally and spatially controlled DSB induction at a defined number of genomic loci: by inducible endonuclease, for example. Followed by chromatin immunoprecipitation (ChIP), this would allow the study of specific protein-DNA interactions (Iacovoni *et al.*, 2010; Aymard *et al.*, 2014).

4.4 Conclusions

To recapitulate, whilst this project failed to find co-operativity between Bleomycin and Benzbromarone in cell proliferation assays, this was likely due to the limitations caused by using a concentration of Benzbromarone more than 4-fold less than that of the IC50; it is improbable that full inhibition of Eya phosphatase was achieved. Nevertheless, this concentration was still found to have some effect in apoptosis assays: using live-cell imaging, a more than 2-fold increase in apoptosis was achieved by co-administrating 25μM of Bleomycin with 8μM of Benzbromarone.

Yet the most intriguing findings of this study have been found through immunochemical staining, whereby di-γH2A.X was found adjacent to, but not co-localising with γH2A.X in DDR foci, appearing to “flank” the γH2A.X signal, as well as interlocking signals of both epigenetic states. In apoptotic cells, an interspersed signal, containing both γH2A.X and di-γH2A.X was found.

This has led to a tentative new model for an additional role of di-γH2A.X, in that it acts in a mechanism in which to control DDR focus expansion, regulated by the Eya phosphotyrosine phosphatase. The proportion of pY142 in resting chromatin and level of Eya phosphatase may therefore act as a "gain control" for the intensity of the DNA damage response in different cell types.

5 References

van Attikum, H. and Gasser, S. M. (2009) 'Crosstalk between histone modifications during the DNA damage response', *Trends in Cell Biology*, 19(5), pp. 207–217. doi: 10.1016/j.tcb.2009.03.001.

Aymard, F., Bugler, B., Schmidt, C. K., Guillou, E., Caron, P., Briois, S., Iacovoni, J. S., Daburon, V., Miller, K. M., Jackson, S. P. and Legube, G. (2014) 'Transcriptionally active chromatin recruits homologous recombination at DNA double-strand breaks.', *Nature structural & molecular biology*. Europe PMC Funders, 21(4), pp. 366–74. doi: 10.1038/nsmb.2796.

Bakkenist, C. J. and Kastan, M. B. (2003) 'DNA damage activates ATM through intermolecular autophosphorylation and dimer dissociation', *Nature*, 421(6922), pp. 499–506. doi: 10.1038/nature01368.

Bao, Y. (2011) 'Chromatin response to DNA double-strand break damage', *Epigenomics*, 3(3), pp. 307–321. doi: 10.2217/epi.11.14.

Bonisch, C. and Hake, S. B. (2012) 'Histone H2A variants in nucleosomes and chromatin: more or less stable?', *Nucleic Acids Research*, 40(21), pp. 10719–10741. doi: 10.1093/nar/gks865.

Botuyan, M. V., Lee, J., Ward, I. M., Kim, J.-E., Thompson, J. R., Chen, J. and Mer, G. (2006) 'Structural Basis for the Methylation State-Specific Recognition of Histone H4-K20 by 53BP1 and Crb2 in DNA Repair', *Cell*, 127(7), pp. 1361–1373. doi: 10.1016/j.cell.2006.10.043.

Bratton, S. B. and Salvesen, G. S. (2010) 'Regulation of the Apaf-1–caspase-9 apoptosome', *Journal of Cell Science*, 123(19). Available at: http://jcs.biologists.org/content/123/19/3209.

Burma, S., Chen, B. P., Murphy, M., Kurimasa, A. and Chen, D. J. (2001) 'ATM Phosphorylates Histone H2A.X in Response to DNA Double-strand Breaks', *Journal of Biological Chemistry*, 276(45), pp. 42462–42467. doi: 10.1074/jbc.C100466200.

Caldecott, K. W. (2007) 'Mammalian single-strand break repair: Mechanisms and links with chromatin', *DNA Repair*, 6(4), pp. 443–453. doi: 10.1016/j.dnarep.2006.10.006.

Campbell, S. J., Edwards, R. A. and Glover, J. N. M. (2010) 'Comparison of the Structures and Peptide Binding Specificities of the BRCT Domains of MDC1 and BRCA1', *Structure*, 18(2), pp. 167–176. doi: 10.1016/j.str.2009.12.008.

Ceballos, S. J. and Heyer, W.-D. (2011) 'Functions of the Snf2/Swi2 family Rad54 motor protein in homologous recombination.', *Biochimica et biophysica acta*. NIH Public Access, 1809(9), pp. 509–23. doi: 10.1016/j.bbagrm.2011.06.006.

Chan, D. W., Chen, B. P.-C., Prithivirajsingh, S., Kurimasa, A., Story, M. D., Qin, J. and Chen, D. J. (2002) 'Autophosphorylation of the DNA-dependent protein kinase catalytic subunit is required for rejoining of DNA double-strand breaks.', *Genes & development*. Cold Spring Harbor Laboratory Press, 16(18), pp. 2333–8. doi: 10.1101/gad.1015202.

Chaurasia, P., Sen, R., Pandita, T. K. and Bhaumik, S. R. (2012) 'Preferential Repair of DNA Double-strand Break at the Active Gene *in Vivo*', *Journal of Biological Chemistry*, 287(43), pp. 36414–36422. doi: 10.1074/jbc.M112.364661.

Chen, W.-T., Alpert, A., Leiter, C., Gong, F., Jackson, S. P. and Miller, K. M. (2013) 'Systematic identification of functional residues in mammalian histone H2A.X.', *Molecular and cellular biology*. American Society for Microbiology (ASM), 33(1), pp. 111–26. doi: 10.1128/MCB.01024-12.

Cheung, W. L., Turner, F. B., Krishnamoorthy, T., Wolner, B., Ahn, S.-H., Foley, M., Dorsey, J. A., Peterson, C. L., Berger, S. L. and Allis, C. D. (2005) 'Phosphorylation of Histone H4 Serine 1 during DNA Damage Requires Casein Kinase II in S. cerevisiae', *Current Biology*, 15(7), pp. 656–660. doi: 10.1016/j.cub.2005.02.049.

Cook, P. J., Ju, B. G., Telese, F., Wang, X., Glass, C. K. and Rosenfeld, M. G. (2009) 'Tyrosine dephosphorylation of H2A.X modulates apoptosis and survival decisions.', *Nature*. NIH Public Access, 458(7238), pp. 591–6. doi: 10.1038/nature07849.

Davis, A. J. and Chen, D. J. (2013) 'DNA double strand break repair via non-homologous end-joining.', *Translational cancer research*. NIH Public Access, 2(3), pp. 130–143. doi: 10.3978/j.issn.2218-676X.2013.04.02.

Dignam, J. D., Lebovitz, R. M. and Roeder, R. G. (1983) 'Accurate transcription initiation by RNA polymerase II in a soluble extract from isolated mammalian nuclei.', *Nucleic acids research*. Oxford University Press, 11(5), pp. 1475–89. Available at: http://www.ncbi.nlm.nih.gov/pubmed/6828386.

Dinant, C., Houtsmuller, A. B. and Vermeulen, W. (2008) 'Chromatin structure and DNA damage repair', *Epigenetics & Chromatin*, 1(1), p. 9. doi: 10.1186/1756-8935-1-9.

Ding, D., Zhang, Y., Wang, J., Zhang, X., Gao, Y., Yin, L., Li, Q., Li, J. and Chen, H. (2016) 'Induction and inhibition of the pan-nuclear gamma-H2A.X response in resting human peripheral blood lymphocytes after X-ray irradiation', *Cell Death Discovery*, 211. doi: 10.1038/cddiscovery.2016.11.

Elmore, S. (2007) ‘Apoptosis: a review of programmed cell death.’, *Toxicologic pathology*. NIH Public Access, 35(4), pp. 495–516. doi: 10.1080/01926230701320337.

Fernandez-Capetillo, O., Allis, C. D. and Nussenzweig, A. (2004) ‘Phosphorylation of histone H2B at DNA double-strand breaks.’, *The Journal of experimental medicine*. The Rockefeller University Press, 199(12), pp. 1671–7. doi: 10.1084/jem.20032247.

van Gent, D. C. and Kanaar, R. (2016) ‘Exploiting DNA repair defects for novel cancer therapies.’, *Molecular biology of the cell*. American Society for Cell Biology, 27(14), pp. 2145–8. doi: 10.1091/mbc.E15-10-0698.

H2AFX (H2A histone family, member X). Available at: http://atlasgeneticsoncology.org/Genes/H2AFXID40783ch11q23.html.

Hargreaves, D. C. and Crabtree, G. R. (2011) ‘ATP-dependent chromatin remodeling: genetics, genomics and mechanisms’, *Cell Research*, 21(3), pp. 396–420. doi: 10.1038/cr.2011.32.

Henikoff, S., Furuyama, T. and Ahmad, K. (2004) ‘Histone variants, nucleosome assembly and epigenetic inheritance’, *Trends in Genetics*, 20(7), pp. 320–326. doi: 10.1016/j.tig.2004.05.004.

Hunt, C. R., Ramnarain, D., Horikoshi, N., Iyengar, P., Pandita, R. K., Shay, J. W. and Pandita, T. K. (2013) ‘Histone modifications and DNA double-strand break repair after exposure to ionizing radiations.’, *Radiation research*. NIH Public Access, 179(4), pp. 383–92. doi: 10.1667/RR3308.2.

Huyen, Y., Zgheib, O., DiTullio Jr, R. A., Gorgoulis, V. G., Zacharatos, P., Petty, T. J., Sheston, E. A., Mellert, H. S., Stavridi, E. S. and Halazonetis, T. D. (2004) 'Methylated lysine 79 of histone H3 targets 53BP1 to DNA double-strand breaks', *Nature*. Nature Publishing Group, 432(7015), pp. 406–411. doi: 10.1038/nature03114.

Iacovoni, J. S., Caron, P., Lassadi, I., Nicolas, E., Massip, L., Trouche, D. and Legube, G. (2010) 'High-resolution profiling of gammaH2A.X around DNA double strand breaks in the mammalian genome.', *The EMBO journal*. European Molecular Biology Organization, 29(8), pp. 1446–57. doi: 10.1038/emboj.2010.38.

Ichim, G. and Tait, S. W. G. (2016) 'A fate worse than death: apoptosis as an oncogenic process', *Nature Reviews Cancer*, 16(8), pp. 539–548. doi: 10.1038/nrc.2016.58.

Iliakis, G., Murmann, T. and Soni, A. (2015) 'Alternative end-joining repair pathways are the ultimate backup for abrogated classical non-homologous end-joining and homologous recombination repair: Implications for the formation of chromosome translocations', *Mutation Research/Genetic Toxicology and Environmental Mutagenesis*, 793, pp. 166–175. doi: 10.1016/j.mrgentox.2015.07.001.

Jeffers, L. J., Coull, B. J., Stack, S. J. and Morrison, C. G. (2008) 'Distinct BRCT domains in Mcph1/Brit1 mediate ionizing radiation-induced focus formation and centrosomal localization', *Oncogene*, 27(1), pp. 139–144. doi: 10.1038/sj.onc.1210595.

Kaufmann, P., Török, M., Hänni, A., Roberts, P., Gasser, R. and Krähenbühl, S. (2005) 'Mechanisms of benzarone and benzbromarone-induced hepatic toxicity', *Hepatology*, 41(4), pp. 925–935. doi: 10.1002/hep.20634.

Kerr, J. F., Wyllie, A. H. and Currie, A. R. (1972) 'Apoptosis: a basic biological phenomenon with wide-ranging implications in tissue kinetics.', *British journal of cancer*, 26(4), pp. 239–57. Available at: http://www.ncbi.nlm.nih.gov/pubmed/4561027.

Khanna, K. K. and Jackson, S. P. (2001) 'DNA double-strand breaks: signaling, repair and the cancer connection', *Nature Genetics*. Nature Publishing Group, 27(3), pp. 247–254. doi: 10.1038/85798.

Kim, Y.-J. and Wilson, D. M. (2012) 'Overview of base excision repair biochemistry.', *Current molecular pharmacology*, 5(1), pp. 3–13. Available at: http://www.ncbi.nlm.nih.gov/pubmed/22122461.

Kinner, A., Wu, W., Staudt, C. and Iliakis, G. (2008) 'γ-H2A.X in recognition and signaling of DNA double-strand breaks in the context of chromatin', *Nucleic Acids Research*, 36(17), pp. 5678–5694. doi: 10.1093/nar/gkn550.

Krishnan, N., Jeong, D. G., Jung, S.-K., Ryu, S. E., Xiao, A., Allis, C. D., Kim, S. J. and Tonks, N. K. (2009) 'Dephosphorylation of the C-terminal tyrosyl residue of the DNA damage-related histone H2A.X is mediated by the protein phosphatase eyes absent.', *The Journal of biological chemistry*. American Society for Biochemistry and Molecular Biology, 284(24), pp. 16066–70. doi: 10.1074/jbc.C900032200.

Li, X. and Heyer, W.-D. (2008) 'Homologous recombination in DNA repair and DNA damage tolerance.', *Cell research*. NIH Public Access, 18(1), pp. 99–113. doi: 10.1038/cr.2008.1.

Li, X., Oghi, K. A., Zhang, J., Krones, A., Bush, K. T., Glass, C. K., Nigam, S. K., Aggarwal, A. K., Maas, R., Rose, D. W. and Rosenfeld, M. G. (2003) 'Eya protein phosphatase activity regulates Six1-Dach-Eya transcriptional effects in mammalian organogenesis.', *Nature*, 426(6964), pp. 247–254. doi: 10.1038/nature02283.

Liu, J.-F., Chen, C.-Y., Chen, H.-T., Chang, C.-S. and Tang, C.-H. (2016) 'BL-038, a Benzofuran Derivative, Induces Cell Apoptosis in Human Chondrosarcoma Cells through Reactive Oxygen Species/Mitochondrial Dysfunction and the Caspases Dependent Pathway', *International Journal of Molecular Sciences*, 17(9), p. 1491.

Lu, C., Zhu, F., Cho, Y.-Y., Tang, F., Zykova, T., Ma, W., Bode, A. M. and Dong, Z. (2006) 'Cell Apoptosis: Requirement of H2A.X in DNA Ladder Formation, but Not for the Activation of Caspase-3', *Molecular Cell*, 23(1), pp. 121–132. doi: 10.1016/j.molcel.2006.05.023.

Luger, K., Dechassa, M. L. and Tremethick, D. J. (2012) 'New insights into nucleosome and chromatin structure: an ordered state or a disordered affair?', *Nature Reviews Molecular Cell Biology*, 13(7), pp. 436–447. doi: 10.1038/nrm3382.

Matsuoka, S., Ballif, B. A., Smogorzewska, A., McDonald, E. R., Hurov, K. E., Luo, J., Bakalarski, C. E., Zhao, Z., Solimini, N., Lerenthal, Y., Shiloh, Y., Gygi, S. P. and Elledge, S. J. (2007) 'ATM and ATR substrate analysis reveals extensive protein networks responsive to DNA damage.', *Science (New York, N.Y.)*. American Association for the Advancement of Science, 316(5828), pp. 1160–6. doi: 10.1126/science.1140321.

Meneghini, M. D., Wu, M. and Madhani, H. D. (2003) 'Conserved histone variant H2A.Z protects euchromatin from the ectopic spread of silent heterochromatin.', *Cell*, 112(5), pp. 725–36. Available at: http://www.ncbi.nlm.nih.gov/pubmed/12628191.

Misteli, T. and Soutoglou, E. (2009) 'The emerging role of nuclear architecture in DNA repair and genome maintenance.', *Nature reviews. Molecular cell biology*. NIH Public Access, 10(4), pp. 243–54. doi: 10.1038/nrm2651.

Mizuguchi, G., Shen, X., Landry, J., Wu, W.-H., Sen, S. and Wu, C. (2004) 'ATP-Driven Exchange of Histone H2AZ Variant Catalyzed by SWR1 Chromatin Remodeling Complex', *Science*, 303(5656), pp. 343–348. doi: 10.1126/science.1090701.

Murphy, T. M., Perry, A. S. and Lawler, M. (2008) 'The emergence of DNA methylation as a key modulator of aberrant cell death in prostate cancer.', *Endocrine-related cancer*. BioScientifica, 15(1), pp. 11–25. doi: 10.1677/ERC-07-0208.

Nagata, S. (2010) 'Apoptosis and autoimmune diseases', *Annals of the New York Academy of Sciences*, 1209(1), pp. 10–16. doi: 10.1111/j.1749-6632.2010.05749.x.

Nagata, S., Enari, M., Sakahira, H., Yokoyama, H., Okawa, K. and Iwamatsu, A. (1998) 'A caspase-activated DNase that degrades DNA during apoptosis, and itsinhibitor ICAD', *Nature*. Nature Publishing Group, 391(6662), pp. 43–50. doi: 10.1038/34112.

Okabe, Y., Sano, T. and Nagata, S. (2009) 'Regulation of the innate immune response by threonine-phosphatase of Eyes absent', *Nature*, 460(7254), pp. 520–4. doi: 10.1038/nature08138.

Ortiz-Bazán, M. Á., Gallo-Fernández, M., Saugar, I., Jiménez-Martín, A., Vázquez, M. V. and Tercero, J. A. (2014) 'Rad5 Plays a Major Role in the Cellular Response to DNA Damage during Chromosome Replication', *Cell Reports*, 9(2), pp. 460–468. doi: 10.1016/j.celrep.2014.09.005.

Pandey, R. N., Rani, R., Yeo, E.-J., Spencer, M., Hu, S., Lang, R. A. and Hegde, R. S. (2010) 'The Eyes Absent phosphatase-transactivator proteins promote proliferation, transformation, migration, and invasion of tumor cells.', *Oncogene*. NIH Public Access, 29(25), pp. 3715–22. doi: 10.1038/onc.2010.122.

Pandey, R. N., Wang, T. Sen, Tadjuidje, E., McDonald, M. G., Rettie, A. E. and Hegde, R. S. (2013) 'Structure-Activity Relationships of Benzbromarone Metabolites and Derivatives as EYA Inhibitory Anti-Angiogenic Agents', *PLoS ONE*. Edited by R. Mohanraj. Public Library of Science, 8(12), p. e84582. doi: 10.1371/journal.pone.0084582.

Park, J.-H., Park, E.-J., Lee, H.-S., Kim, S. J., Hur, S.-K., Imbalzano, A. N. and Kwon, J. (2006) 'Mammalian SWI/SNF complexes facilitate DNA double-strand break repair by promoting ?-H2A.X induction', *The EMBO Journal*, 25(17), pp. 3986–3997. doi: 10.1038/sj.emboj.7601291.

Petrini, J. H. J. and Stracker, T. H. (2003) 'The cellular response to DNA double-strand breaks: defining the sensors and mediators.', *Trends in cell biology*. Elsevier, 13(9), pp. 458–62. doi: 10.1016/S0962-8924(03)00170-3.

Pilch, D. R., Sedelnikova, O. A., Redon, C., Celeste, A., Nussenzweig, A. and Bonner, W. M. (2003) 'Characteristics of γ-H2A.X foci at DNA double-strand breaks sites', *Biochemistry and Cell Biology*. NRC Research Press Ottawa, Canada , 81(3), pp. 123–129. doi: 10.1139/o03-042.

Polo, S. E. and Jackson, S. P. (2011) 'Dynamics of DNA damage response proteins at DNA breaks: a focus on protein modifications.', *Genes & development*. Cold Spring Harbor Laboratory Press, 25(5), pp. 409–33. doi: 10.1101/gad.2021311.

Rayapureddi, J. P., Kattamuri, C., Chan, F. H. and Hegde, R. S. (2005) 'Characterization of a Plant, Tyrosine-Specific Phosphatase of the Aspartyl Class', *Biochemistry*, 44(2), pp. 751–758. doi: 10.1021/bi0481794.

Rayapureddi, J. P., Kattamuri, C., Steinmetz, B. D., Frankfort, B. J., Ostrin, E. J., Mardon, G. and Hegde, R. S. (2003) 'Eyes absent represents a class of protein tyrosine phosphatases', *Nature*, 426(6964), pp. 295–298. doi: 10.1038/nature02093.

Rebay, I. (2015) 'Multiple Functions of the Eya Phosphotyrosine Phosphatase.', *Molecular and cellular biology*. American Society for Microbiology (ASM), 36(5), pp. 668–77. doi: 10.1128/MCB.00976-15.

Rogakou, E. P., Boon, C., Redon, C. and Bonner, W. M. (1999) 'Megabase chromatin domains involved in DNA double-strand breaks in vivo.', *The Journal of cell biology*, 146(5), pp. 905–16. Available at: http://www.ncbi.nlm.nih.gov/pubmed/10477747.

Rogakou, E. P., Nieves-Neira, W., Boon, C., Pommier, Y. and Bonner, W. M. (2000) 'Initiation of DNA fragmentation during apoptosis induces phosphorylation of H2A.X histone at serine 139.', *The Journal of biological chemistry*. American Society for Biochemistry and Molecular Biology, 275(13), pp. 9390–5. doi: 10.1074/JBC.275.13.9390.

Rogakou, E. P., Pilch, D. R., Orr, A. H., Ivanova, V. S. and Bonner, W. M. (1998) 'DNA double-stranded breaks induce histone H2A.X phosphorylation on serine 139.', *The Journal of biological chemistry*, 273(10), pp. 5858–68. Available at: http://www.ncbi.nlm.nih.gov/pubmed/9488723.

Scarpato, R., Castagna, S., Aliotta, R., Azzara, A., Ghetti, F., Filomeni, E., Giovannini, C., Pirillo, C., Testi, S., Lombardi, S. and Tomei, A. (2013) 'Kinetics of nuclear phosphorylation (γ-H2A.X) in human lymphocytes treated in vitro with UVB, bleomycin and mitomycin C', *Mutagenesis*. Oxford University Press, 28(4), pp. 465–473. doi: 10.1093/mutage/get024.

Schärer, O. D. (2013) 'Nucleotide excision repair in eukaryotes.', *Cold Spring Harbor perspectives in biology*. Cold Spring Harbor Laboratory Press, 5(10), p. a012609. doi: 10.1101/cshperspect.a012609.

Shroff, R., Arbel-Eden, A., Pilch, D., Ira, G., Bonner, W. M., Petrini, J. H., Haber, J. E. and Lichten, M. (2004) 'Distribution and Dynamics of Chromatin Modification Induced by a Defined DNA Double-Strand Break', *Current Biology*, 14(19), pp. 1703–1711. doi: 10.1016/j.cub.2004.09.047.

Singh, N., Basnet, H., Wiltshire, T. D., Mohammad, D. H., Thompson, J. R., Héroux, A., Botuyan, M. V., Yaffe, M. B., Couch, F. J., Rosenfeld, M. G. and Mer, G. (2012) 'Dual recognition of phosphoserine and phosphotyrosine in histone variant H2A.X by DNA damage response protein MCPH1.', *Proceedings of the National Academy of Sciences of the United States of America*. National Academy of Sciences, 109(36), pp. 14381–6. doi: 10.1073/pnas.1212366109.

So, S., Davis, A. J. and Chen, D. J. (2009) 'Autophosphorylation at serine 1981 stabilizes ATM at DNA damage sites', *The Journal of Cell Biology*, 187(7). Available at: http://jcb.rupress.org/content/187/7/977.

Solier, S., Kohn, K. W., Scroggins, B., Xu, W., Trepel, J., Neckers, L. and Pommier, Y. (2012) 'Heat shock protein 90 (HSP90), a substrate and chaperone of DNA-PK necessary for the apoptotic response', *Proceedings of the National Academy of Sciences*, 109(32), pp. 12866–12872. doi: 10.1073/pnas.1203617109.

Solier, S. and Pommier, Y. (2009) ‘The apoptotic ring: A novel entity with phosphorylated histones H2A.X and H2B, and activated DNA damage response kinases’, *Cell Cycle*, 8(12), pp. 1853–1859. doi: 10.4161/cc.8.12.8865.

Solier, S. and Pommier, Y. (2011) ‘MDC1 Cleavage by Caspase-3: A Novel Mechanism for Inactivating the DNA Damage Response during Apoptosis’, *Cancer Research*, 71(3), pp. 906–913. doi: 10.1158/0008-5472.CAN-10-3297.

Solier, S. and Pommier, Y. (2014) ‘The nuclear γ-H2A.X apoptotic ring: implications for cancers and autoimmune diseases’, *Cellular and Molecular Life Sciences*, 71(12), pp. 2289–2297. doi: 10.1007/s00018-013-1555-2.

Spycher, C., Miller, E. S., Townsend, K., Pavic, L., Morrice, N. A., Janscak, P., Stewart, G. S. and Stucki, M. (2008) ‘Constitutive phosphorylation of MDC1 physically links the MRE11–RAD50–NBS1 complex to damaged chromatin’, *The Journal of Cell Biology*, 181(2), pp. 227–240. doi: 10.1083/jcb.200709008.

Stewart, G. S., Wang, B., Bignell, C. R., Taylor, A. M. R. and Elledge, S. J. (2003) ‘MDC1 is a mediator of the mammalian DNA damage checkpoint’, *Nature*. Nature Publishing Group, 421(6926), pp. 961–966. doi: 10.1038/nature01446.

Stucki, M., Clapperton, J. A., Mohammad, D., Yaffe, M. B., Smerdon, S. J. and Jackson, S. P. (2005) ‘MDC1 Directly Binds Phosphorylated Histone H2A.X to Regulate Cellular Responses to DNA Double-Strand Breaks’, *Cell*, 123(7), pp. 1213–1226. doi: 10.1016/j.cell.2005.09.038.

Tadjuidje, E., Wang, T. Sen, Pandey, R. N., Sumanas, S., Lang, R. A. and Hegde, R. S. (2012) ‘The EYA tyrosine phosphatase activity is pro-angiogenic and is inhibited by benzbromarone.’, *PloS one*. Public Library of Science, 7(4), p. e34806. doi: 10.1371/journal.pone.0034806.

Taylor, R. C., Cullen, S. P. and Martin, S. J. (2008) ‘Apoptosis: controlled demolition at the cellular level’, *Nature Reviews Molecular Cell Biology*, 9(3), pp. 231–241. doi: 10.1038/nrm2312.

Torgovnick, A. and Schumacher, B. (2015) ‘DNA repair mechanisms in cancer development and therapy.’, *Frontiers in genetics*. Frontiers Media SA, 6, p. 157. doi: 10.3389/fgene.2015.00157.

Turinetto, V. and Giachino, C. (2015) ‘Multiple facets of histone variant H2A.X: a DNA double-strand-break marker with several biological functions.’, *Nucleic acids research*, 43(5), pp. 2489–98. doi: 10.1093/nar/gkv061.

Uchida, S., Shimada, K., Misaka, S., Imai, H., Katoh, Y., Inui, N., Takeuchi, K., Ishizaki, T., Yamada, S., Ohashi, K., Namiki, N. and Watanabe, H. (2010) ‘Benzbromarone pharmacokinetics and pharmacodynamics in different cytochrome P450 2C9 genotypes.’, *Drug metabolism and pharmacokinetics*, 25(6), pp. 605–10. Available at: http://www.ncbi.nlm.nih.gov/pubmed/20962433.

Varmark, H., Sparks, C. A., Nordberg, J. J., Koppetsch, B. S. and Theurkauf, W. E. (2009) ‘DNA damage-induced cell death is enhanced by progression through mitosis.’, *Cell cycle (Georgetown, Tex.)*. NIH Public Access, 8(18), pp. 2951–63. Available at: http://www.ncbi.nlm.nih.gov/pubmed/19713770.

de Vries, J. X., Walter-Sack, I., Ittensohn, A., Weber, E., Empl, H., Gresser, U. and Zöllner, N. (1993) ‘Benzbromarone hydroxylation in man: defective formation of the 6-hydroxybenzbromarone metabolite.’, *The Clinical investigator*, 71(11), pp. 947–52. Available at: http://www.ncbi.nlm.nih.gov/pubmed/8312690.

Wachmann, K., Pop, C., van Raam, B. J., Drag, M., Mace, P. D., Snipas, S. J., Zmasek, C., Schwarzenbacher, R., Salvesen, G. S. and Riedl, S. J. (2010) 'Activation and specificity of human caspase-10.', *Biochemistry*. NIH Public Access, 49(38), pp. 8307–15. doi: 10.1021/bi100968m.

Walter-Sack, I., de Vries, J. X., Ittensohn, A. and Weber, E. (1990) 'Rapid and slow benzbromarone elimination phenotypes in man: benzbromarone and metabolite profiles.', *European journal of clinical pharmacology*, 39(6), pp. 577–81. Available at: http://www.ncbi.nlm.nih.gov/pubmed/2095343.

Wood, J. L., Singh, N., Mer, G. and Chen, J. (2007) 'MCPH1 Functions in an H2A.X-dependent but MDC1-independent Pathway in Response to DNA Damage', *Journal of Biological Chemistry*, 282(48), pp. 35416–35423. doi: 10.1074/jbc.M705245200.

Xiao, A., Li, H., Shechter, D., Ahn, S. H., Fabrizio, L. A., Erdjument-Bromage, H., Ishibe-Murakami, S., Wang, B., Tempst, P., Hofmann, K., Patel, D. J., Elledge, S. J. and Allis, C. D. (2009) 'WSTF regulates the H2A.X DNA damage response via a novel tyrosine kinase activity', *Nature*, 457(7225), pp. 57–62. doi: 10.1038/nature07668.

Xiong, W., Dabbouseh, N. M. and Rebay, I. (2009) 'Interactions with the Abelson Tyrosine Kinase Reveal Compartmentalization of Eyes Absent Function between Nucleus and Cytoplasm', *Developmental Cell*, 16(2), pp. 271–279. doi: 10.1016/j.devcel.2008.12.005.

You, Z., Chahwan, C., Bailis, J., Hunter, T. and Russell, P. (2005) 'ATM Activation and Its Recruitment to Damaged DNA Require Binding to the C Terminus of Nbs1', *Molecular and Cellular Biology*, 25(13), pp. 5363–5379. doi: 10.1128/MCB.25.13.5363-5379.2005.

Zhao, Y., Sui, X. and Ren, H. (2010) ‘From procaspase-8 to caspase-8: Revisiting structural functions of caspase-8’, *Journal of Cellular Physiology*, 225(2), pp. 316–320. doi: 10.1002/jcp.22276.

Zhu, F., Zykova, T. A., Peng, C., Zhang, J., Cho, Y.-Y., Zheng, D., Yao, K., Ma, W.-Y., Lau, A. T. Y., Bode, A. M. and Dong, Z. (2011) ‘Phosphorylation of H2A.X at Ser139 and a New Phosphorylation Site Ser16 by RSK2 Decreases H2A.X Ubiquitination and Inhibits Cell Transformation’, *Cancer Research*, 71(2). Available at: http://cancerres.aacrjournals.org/content/71/2/393.

6 Supplementary data

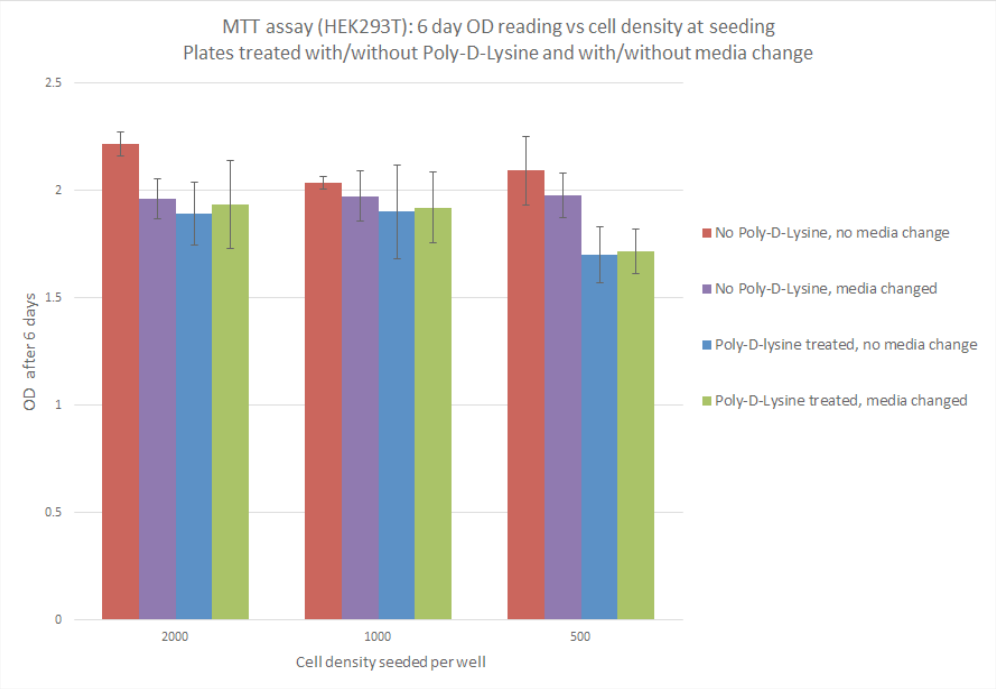

Figure 6-1 The effect of Poly-D-Lysine on cell proliferation

HEK293T cells seeded in untreated plates with no media change had the highest viability; in comparison, cell viability was lower in untreated plates when the media was changed, indicating loss of cells during media change through lack of adherence. Cells in Poly-D-Lysine treated plates with no media change had lower viability than untreated plates with no media change, indicating Poly-D-Lysine has some toxicity to 293T cells. However, no difference was seen between Poly-D-Lysine treated cells with/without media change, indicating cells were not lost through media change. HEK293T cells were seeded in triplicate repeats in a 96-well plate, at either 2000, 1000 or 500 cells per well. 96-well plates were either untreated, or treated with Poly-D-Lysine and then washed twice with dH_20 and once with 96% ethanol prior to seeding. After 24-hrs, media was changed on the plates indicated. Cells were incubated for 5-days before addition of MTT and absorbance read on a plate-reader at 570nm. Error bars based on SD of the triplicate repeats.

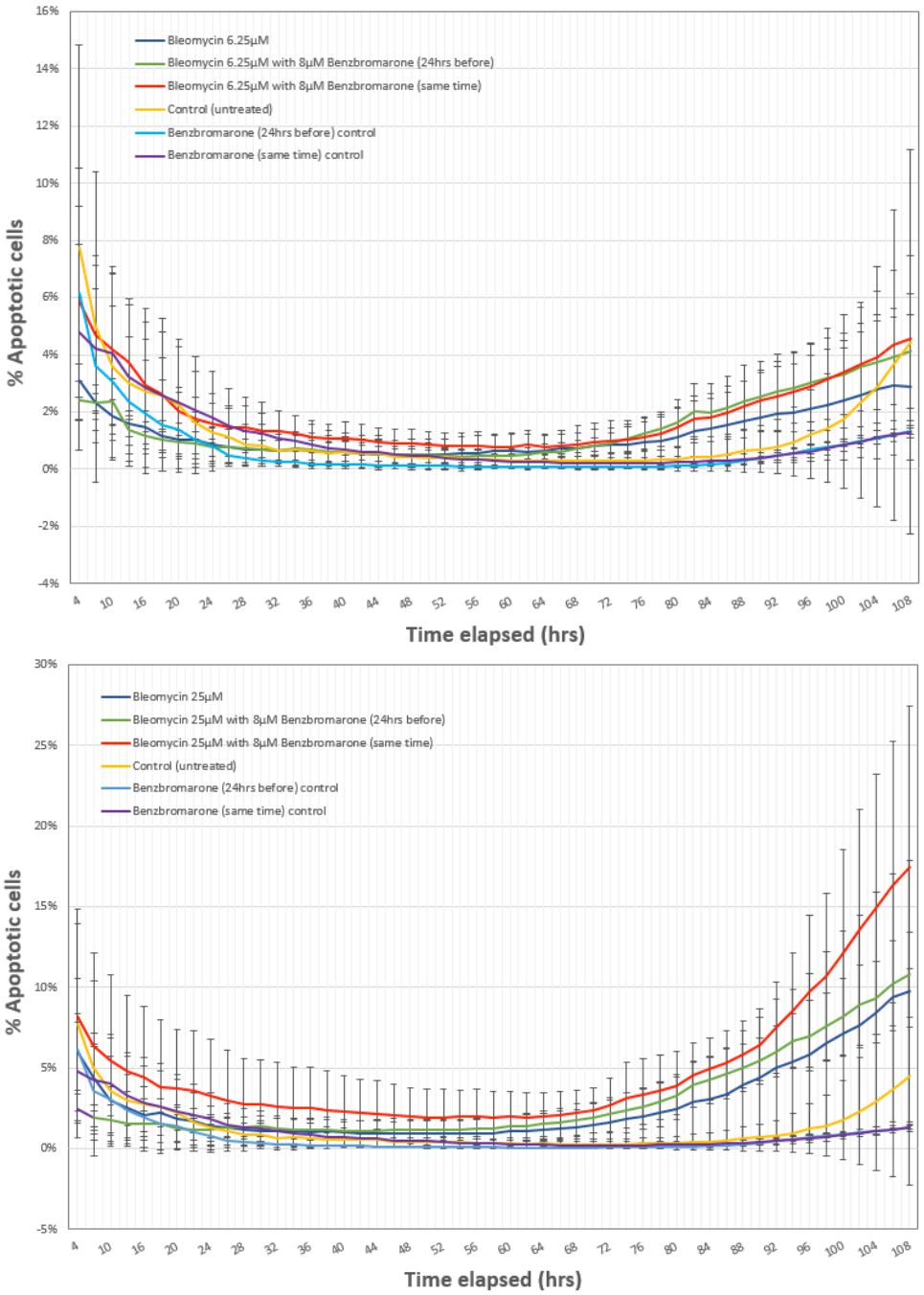

Figure 6-2 Co-operativity between Benzbromarone and a pulse treatment of Bleomycin, by cleaved caspase-3/7 detection

Co-treatment of Bleomycin with 8µM of Benzbromarone increases apoptosis. HEK293T cells were seeded in quadruple repeats in treated 96-well plates, 2000 cells per well, with/without 8µM Benzbromarone. 24hrs later, cells were treated with a serial dilution of Bleomycin which was removed after 2-hrs and replaced with fresh media, with/without 8µM of Benzbromarone and incubated with Caspase 3/7 reagent in an IncuCyte Live-Cell Analysis System. Cell growth and apoptosis was monitored, capturing 4 images per well, every 2 hrs at 10x objective for 106-hrs.